

1 **Age and geochemistry of tephra layers from Ischia, Italy: constraints from proximal-**
2 **distal correlations with Lago Grande di Monticchio**

3

4 **Emma L. Tomlinson^{1*}, Paul G. Albert^{1,^}, Sabine Wulf², Richard J. Brown³, Victoria C.**
5 **Smith⁴, Jörg Keller⁵, Giovanni Orsi⁷, Anna J. Bourne^{8^}, Martin A. Menzies¹**

6

7 ¹Department of Earth Sciences, Royal Holloway University of London, Egham, UK

8 ²GFZ German Research Centre for Geosciences, Section 5.2 – Climate Dynamics and Landscape Evolution,
9 Potsdam, Germany

10 ³Department of Earth Sciences, Science Labs, Durham University, Durham, UK

11 ⁴Research Laboratory for Archaeology and the History of Art, University of Oxford, Oxford, UK

12 ⁵Institute of Geosciences, Mineralogy and Geochemistry, Albert-Ludwigs-University Freiburg, Freiburg,
13 Germany

14 ⁷Instituto Nazionale di Geofisica e Vulcanologia, Sezione di Napoli-Osservatorio Vesuviano, Napoli, Italy.

15 ⁸Centre of Quaternary Research, Department of Geography, Royal Holloway University of London, Egham,
16 UK

17

18 *Present address: Department of Geology, Trinity College Dublin, Dublin, Ireland

19 ^Present address: Department of Geography, College of Science, Swansea University, Swansea, UK.

20

21 **Corresponding author: tomlinse@tcd.ie**

22

23 **Abstract**

24 Unraveling the eruptive history of the Island of Ischia (southern Italy) is problematic due its
25 to burial, caldera collapse, resurgent uplift and erosion. Here, we present new major and
26 trace element glass data for 39-75 ka proximal tephra deposits, including the caldera-
27 forming Monte Epomeo Green Tuff (MEGT) eruption. Correlations with the distal tephra
28 archive preserved at Lago Grande di Monticchio (LGdM) are used to constrain the timing of
29 yet undated eruptive events. Out of 13 LGdM tephra analysed from the 39-104 ka time
30 window, glass geochemical data show all are compositionally consistent with explosive

31 volcanism erupted on Ischia, whilst 5 of these could be correlated with specific proximal
32 deposits..

33

34 Pre-MEGT pyroclastic sequences comprise three compositional groups, these groups occur
35 repeatedly in successive eruptions. Proximal-distal correlations indicate that the Porticello
36 and Tisichiello eruptions occurred at 76 ± 3 ka and 59 ± 2 ka, respectively. The MEGT
37 eruption is correlated with LGdM TM-19, which has been directly dated at 55 ± 2 ka. Post-
38 MEGT tephras form compositional groups that overlap with the pre-MEGT but are displaced
39 to lower FeO and TiO₂ and lower incompatible element contents. Proximal-distal
40 correlations indicate that the Schiappone and Pietre Rosse eruptions occurred at 50.6 ± 2.0
41 ka and 45 ± 6 ka, respectively.

42

43 Tephra from the MEGT eruption span a wide compositional range, broadly overlapping the
44 three pre-MEGT compositional groups but are displaced to higher Nd and Y and contain an
45 additional less evolved glass population. Glass geochemistry is used to recognise and
46 confirm distal equivalents of the MEGT at LGdM (TM-19) and in the Ionian (Y-7), Adriatic
47 (PRAD 1870) and Tyrrhenian (C-18, MD 28) seas. Distal occurrences of MEGT tephra
48 define a dispersal axis to the south-southeast and are found as far as 540 km from Ischia,
49 making MEGT one of the most widely dispersed late Quaternary pyroclastic deposit erupted
50 in the Campanian region. We have estimated a volume of approximately 40 km³ for the
51 fallout portion of the MEGT pyroclastic sequence on the basis of proximal and distal deposit
52 thicknesses.

53

54 **Keywords:** tephrochronology; volcanic ash; Ischia; explosive eruptions; quaternary
55 volcanism; Campanian volcanic field

56

57 **1. Introduction**

58 Knowledge of past eruptive behaviour is critical for volcanic hazard assessment and for
59 defining future eruption scenarios. Distal tephra archives can provide valuable information
60 about eruptive histories, as well as information about the long-term chemical evolution of a
61 volcanic-magmatic system. This is particularly useful in cases where unravelling eruptive
62 history from proximal deposits is problematic, for example where outcrop is limited by poor
63 exposure or where the stratigraphic record is incomplete due to erosion or deposition at
64 sea, such as is common at island volcanoes (e.g., Brown and Branney 2013; Cassidy et al.,
65 2014).

66
67 The volcanic island of Ischia, southern Italy, has been characterised by alternating periods
68 of intense volcanic activity, resurgence, and quiescence (Orsi et al. 1991; 1996; de Vita et
69 al., 2006) since ca.150 ka (Poli et al., 1987; Gillot et al. 1982; Vezzoli 1988). The largest
70 eruption was the 56 ka (Gillot et al., 1982) caldera-forming Monte Epomeo Green Tuff
71 (MEGT). Much of the present knowledge about Ischia's volcanic past has come from study
72 of proximal deposits, which are incomplete, poorly exposed and heavily eroded (e.g., Brown
73 et al., 2008). Located one hundred and fifty kilometres to the east of Ischia, the annually
74 laminated (varved) sediments of Lago Grande di Monticchio (LGdM; Fig. 1) span 3-133 ka
75 and provide a key tephra archive of volcanism in the region (Wulf et al., 2004). LGdM is
76 ideally positioned along the dominant downwind dispersal axes of volcanic plumes from the
77 Phlegraean Volcanic District and numerous tephra layers in the LGdM record have been
78 attributed to Ischia (Wulf et al., 2008; 2012). From a hazard assessment perspective, this
79 same dispersal axis passes over the now heavily populated city of Naples. The LGdM
80 sedimentary record provides a precise stratigraphy and independent (varve) chronology,
81 which is essential for constraining the eruptive history of Ischia. Explosive activity at Ischia
82 has produced several important widespread tephra markers that were dispersed widely
83 across the Tyrrhenian, Ionian and Adriatic seas (e.g. Keller et al., 1978; Paterne et al.,
84 1988; Tamburino, 2008; Bourne et al., 2010). These include the Y-7 tephra from the Ionian

85 Sea (Keller et al., 1978) and the C-18, C-17 and C-16 layers from the Tyrrhenian Sea
86 (Paterne et al., 1986, 1988). The C-17 tephra has been correlated with the MEGT eruption
87 (Paterne et al., 1986, 1988), while Y-7 was previously linked to an older Ischia eruption, the
88 Sant'Angelo Tephra (Keller et al., 1978; Wulf et al., 2004). However, Paterne et al. (1988)
89 linked the C-18 layer to the Y-7 layer, and this highlights some of the uncertainty as to the
90 correlations and age of these marker tephra.

91

92 In this contribution, we provide micron-beam major and trace element data for Ischia
93 glasses from proximal tephra outcrops, this data is essential for precisely assigning distal
94 tephra to explosive activity at Ischia. Furthermore, we also present multi-elemental glass
95 data from suspected Ischia distal tephra layers recorded within the LGdM tephra record,
96 and other key distal localities in the Ionian and Adriatic Seas. The distal tephra layers
97 investigated here span 104-39 ka and record volcanic eruptions that are likely to be found in
98 other sedimentary archives across the Mediterranean. We define diagnostic geochemical
99 fingerprints for key Ischia tephra layers and provide proximal-distal correlations for a
100 number of important eruptions. The correlations defined herein are used to: 1) constrain the
101 ages eruptions at Ischia; 2) assess the temporal variation in the composition of Ischia
102 products; and 3) evaluate the dispersal axis of the MEGT and calculate the volume of the
103 fall component.

104

105 **2. Background**

106 The volcanic island of Ischia, located in the Tyrrhenian Sea, at the northwestern corner of
107 the Bay of Naples, is the most westerly volcano in the Phlegraean Volcanic District, which
108 also includes Campi Flegrei and Procida–Vivara. Ischia is a caldera with a complex volcanic
109 and structural history. The oldest dated rocks on the Island are a series of lava flows, tuffs
110 and scoria cones erupted at 150 ka (Poli et al., 1987; Gillot et al. 1982; Vezzoli 1988),
111 however magnetic data indicate that Ischia is the remnant of an older, larger volcanic

112 complex extending to the west of the island (Orsi et al. 1999; Bruno et al. 2002). The 7 x 10
113 km caldera was formed during the 56 ka MEGT eruption (Gillot et al., 1982). The centre of
114 the caldera has been uplifted by resurgence to a height of 789 m above sea level over the
115 past 30 ka, forming the Monte Epomeo resurgent block. The most recent eruption was in
116 1302 AD and on-going earthquakes, thermal springs and fumarolic activity (Buchner et al.,
117 1996; Di Napoli et al., 2009, 2011 and references therein) indicate that Ischia is still active.
118 Erupted magmas are dominantly alkali-trachytes, with subordinate shoshonite, latite and
119 phonolite (Poli et al., 1987; Crisci et al., 1989; Civetta et al., 1991; Piochi et al., 1999).

120

121 Volcanic activity at Ischia is characterised by alternating periods of resurgence, intense
122 volcanic activity and quiescence (Orsi et al. 1991; 1996; de Vita et al., 2006; Vezzoli et al.,
123 2009), with Post-MEGT activity occurring in three cycles (55 – 33 ka; 28 – 18 ka; 10 ka –
124 1302 AD; Civetta et al., 1991). The period of interest for this study spans 75-39 ka, starting
125 at the time at which explosive activity began at Ischia, at ~ 75 ka BP. We include the
126 caldera-forming MEGT eruption and the oldest succeeding explosive eruptions of the first
127 cycle (55 – 33 ka) identified by Civetta et al. (1991).

128

129 The 75-60 ka period was dominated by intense explosive volcanic activity characterized by
130 numerous magmatic and phreatomagmatic eruptions (Brown et al., 2008; Sbrana et al.,
131 2009). The eruptions were fed by phono-trachytic magmas and their deposits, include the
132 Sant'Angelo Tephra, Olummo, Tisichiello and Porticello units of Brown et al. (2008).

133

134 The 55-33 ka cycle of activity of Civetta et al. (1991) began with the caldera-forming
135 eruption of the Monte Epomeo Green Tuff (MEGT) (Vezzoli 1988; Tibaldi and Vezzoli 1998;
136 Brown et al., 2008). The MEGT was fed by the compositionally most variable of the Ischia
137 magmas. Post-MEGT activity, extruded trachytic to latitic magmas, and comprised
138 magmatic and phreatomagmatic eruptions that generated the fallout and pyroclastic density

139 current (PDC) deposits. These include the Schiappone unit of Brown et al. (2008), and the
140 Pietre Rosse, and Agnone units of Civetta et al. (1991).

141

142 **3. Samples**

143 **3.1 Proximal samples**

144 Herein, we have focused on the eruptions that are likely to have led to the widespread
145 dispersal of tephra. The investigated eruptions are those that have produced (from oldest to
146 youngest) the Pre-MEGT Sant'Angelo Tephra, Olummo Tephra, Tisichiello Tephra,
147 Porticello tephra, and MEGT (Brown et al., 2008), and Post-MEGT Schiappone Tephra
148 (Brown et al., 2008), Pietre Rosse Tuff and Agnone Tuff (Civetta et al., 1991). The sampled
149 localities are shown in figure 1b.

150

151 The Sant'Angelo Tephra sequence (termed the Unità di Monte Sant'Angelo (UMSA) by Rosi
152 et al. 1988) is a series of decimetre thick pumice fall deposits and ignimbrites overlain by
153 block and ash flow deposits (Brown et al., 2008). The Sant'Angelo Tephra is limited to one
154 outcrop in the south of Ischia, leading Brown et al. (2008) to suggest that they formed as a
155 result of small-volume explosive and effusive eruptions. It has been interpreted as a
156 precursor to, or the first distinct phase of, the MEGT cycle (Rosi et al., 1988; Vezzoli, 1988;
157 Morche 1988; Wulf et al. 2004; Kraml 1997). The position of the Sant'Angelo Tephra relative
158 the Olummo, Tisichiello and Porticello tephtras is not known as they are not found together
159 in stratigraphic section (Brown et al., 2008; Table 1).

160

161 The Olummo, Tisichiello and Porticello tephtras are a succession of 3.5 to >7 m thick
162 bedded pumice and ash fall deposits separated by paleosols (Brown et al., 2008), these are
163 classified as the deposits of sub-Plinian eruptions (Brown et al., 2014). A block-and-ash flow
164 deposit caps the Olummo Tephra (Brown et al., 2008). The Olummo, Tisichiello and
165 Porticello tephtras form part of the Pignatiello Formation of Forcella et al. (1982) and Vezzoli

166 (1988) and overlying the scoria breccia of the 74 ka Parata formation (Vezzoli et al., 1988).

167

168 MEGT pumice fall deposits exceed 8 m thick are exposed in extracaldera locations along
169 the southern coast of Ischia. They are overlain by ignimbrites and lithic breccias that can be
170 traced to Procida and western Campi Flegrei (Brown et al., 2008). The lower ignimbrite is
171 ~70 m thick, while the upper ignimbrite reaches 200 m thick. They are separated by vitric
172 siltstone and sandstone that indicate a hiatus during the eruption (Brown et al., 2008). K-Ar
173 age determinations for the intracaldera ignimbrite range from 51 ka to 59 ka, excluding
174 those with large errors (Gillot et al., 1982).

175

176 The Schiappone tephra comprises a 7 m pumice fall deposit intercalated with ignimbrites
177 and is likely to represent Plinian activity (Brown et al., 2014). This is overlain by a >60 m
178 thick massive ignimbrite (Brown et al., 2008). The Schiappone tephra was previously
179 interpreted as extracaldera deposits of the MEGT (Rosi et al. 1988; Vezzoli 1988). K-Ar
180 age determinations for the Schiappone tephra range from 48-52 ka (Vezzoli 1988, for units
181 previously correlated with the MEGT).

182

183 The Pietre Rosse and Agnone tuff units are exposed in the southwest and northwest
184 corners of Ischia and comprise bedded pumiceous tuffs with interbedded cross-stratified
185 ignimbrites (Civetta et al., 1991). K-Ar dating indicates ages of 44-48 ka and 39-45 ka for
186 the Pietre Rosse and Agnone tuffs, respectively (Poli et al., 1987). These deposits were
187 collectively termed the Citara-Serrara Fontana Formation by Rittmann (1930).

188

189 The characteristics of all samples investigated, including colour and mineral assemblages,
190 are summarised in table 1. Samples below and including Schiappone are described and
191 stratigraphic columns are presented in Brown et al. (2008; 2014), whilst Pietre Rosse and
192 Agnone tuff samples follow Brown et al. (2008; 2014) and Civetta et al. (1991).

194 **3.2 Distal samples**

195 *3.2.1 Lago Grande di Monticchio (LGdM)*

196 The laminated sediments at LGdM (Fig.1a) provide a high-precision varve age and
197 sedimentation rate record (Brauer et al., 2007) with an incremental counting error on LGdM
198 varve ages of 5-10 % (Wulf et al., 2012). We have determined the major and trace element
199 concentrations of 13 tephra layers in the LGdM core, that are thought to have originated
200 from Ischia between 39 and 104 ka BP (Table 2). We focus on tephra layers that are > 1mm
201 thick, these layers include TM-19 and TM-20, that were previously correlated to the MEGT
202 and Sant'Angelo Tephra, respectively (Wulf et al., 2004).

203

204 *3.2.2 Stromboli Island (Aeolian Islands)*

205 Exotic volcanic deposits on the Aeolian Islands provide a useful record of major ash
206 dispersals sourced from the Italian mainland and, in particular, from the Campanian region
207 (Keller 1981; Morche 1988). The '*Ischia tephra*' layer was first recognised on the Island of
208 Salina (Keller 1969), but also outcrops on Filicudi, Lipari, Panarea and Stromboli (Keller
209 1969, 1980; Morche 1988; Lucchi et al., 2008). On the island of Stromboli the tephra layer
210 occurs on the eastern lower flank of the volcano and is referred to as the '*Ischia tephra*
211 *Stromboli*' (ITS) (Morche 1988; Hornig-Kjarsgaard et al. 1993; Kraml 1997). Following
212 Morche (1988) and Hornig-Kjarsgaard et al. (1993), this yellow ash layer on Stromboli is up
213 to 25-30 cm thick and is inter-bedded within locally derived scoriaceous lapilli deposits. The
214 tephra of our sample ITS contained K-feldspar, biotite, plagioclase, clinopyroxene and the
215 key index minerals titanite (sphene, CaTiSiO_5) and yellow acmite in order of decreasing
216 abundance. The ITS tephra on Stromboli has been directly dated by $^{40}\text{Ar}/^{39}\text{Ar}$ analyses of
217 sanidine grains to 56 ± 4 ka (Kraml, 1997).

218

219 *3.2.3 M25/4-11 (Ionian Sea)*

220 Four piston cores (M25/4-10 to 13) were retrieved in 1993 from the Calabrian Rise (36.7542
221 N; 17.1806 E) in the Ionian Sea as part of a specific tephrochronology project during cruise
222 M25 of R/V *Meteor* (Keller 1994). All four cores contained the Y-7 tephra layer in the Y-zone
223 in stratigraphic sequence. The studied Y-7 tephra was retrieved in piston core M25/4-11
224 (36.7542 N; 17.1806 E). The Y-7 tephra occurs at a depth of 223-225 cm, above but close
225 to the MIS 3/4 transition (Keller 1978; Negri et al. 1999; Kraml, 1997). The Y-7 tephra layer
226 contains K-feldspar, biotite, plagioclase, clinopyroxene, titanite and acmite, in a decreasing
227 order of abundance. The astronomically calibrated sapropel chronology and the oxygen
228 isotope chronology give interpolated ages of ca. 50 ka for the Y-7 tephra (Kraml 1997; Negri
229 et al. 1999).

230

231 *3.2.4 PRAD 1-2 (Adriatic Sea)*

232 PRAD 1-2 was recovered from the western and upper flank of the Mid-Adriatic deep
233 (42.6763 N; 14.7704 E) at 185.5 m water depth (Bourne et al., 2010). The cryptotephra
234 layer PRAD-1870 was identified at 1870 cm depth and stratigraphically lies above the MIS
235 3/4 transition. The glass shards are typically platy and colourless (Bourne et al. 2010).

236

237 **4. Analytical Methods**

238 Proximal pumice clasts were crushed and clean fragments from the interiors of up to thirty
239 individual clasts were picked and mounted in 'Stuers EpoFix' epoxy resin for analysis.
240 Individual shards of distal tephra were also mounted in Stuers EpoFix for geochemical
241 micro-beam analysis.

242

243 **4.1 Electron Micro-Probe Analysis (EMPA)**

244 Major element concentrations of individual glass shards of proximal and distal tephra
245 samples were determined using JEOL JXA-8600 electron microprobe, equipped with 4
246 spectrometers and SamX software, at the Research Laboratory for Archaeology and the

247 History of Art, University of Oxford. An accelerating voltage of 15 kV, low beam current (6
248 nA), and defocused (10 μm) beam were used to minimize Na migration. Count times were
249 30 s on each peak, except for Na (10 s) and P and Cl (60 s). The instrument was calibrated
250 for each set of beam conditions using a suite of appropriate mineral standards. The
251 calibration was verified using a range of secondary glass standards from the Max Planck
252 Institute. Count rates were corrected using the PAP absorption correction method. Sample
253 totals are normalised to 100 wt% in all plots and tables. Analytical precision is <10% relative
254 standard deviation (%RSD) for analyses with concentrations >0.8 wt%. Error bars on plots
255 represent the 2x standard deviation of replicate analyses of MPI-DING StHs6/80-G.

256

257 ***4.2 Laser Ablation Inductively Coupled Plasma Mass Spectrometry (LA-ICP-MS)***

258 LA-ICP-MS analyses of glass shards of proximal and distal tephra were performed using an
259 Agilent 7500es coupled to a Resonetics 193 nm ArF excimer laser-ablation system
260 (RESOLUTION M-50 prototype) with a two-volume ablation cell (Muller et al., 2009) at the
261 Department of Earth Sciences, Royal Holloway University of London. We used 34, 25 and
262 20 μm laser spots, depending on the size of the area available for analysis in different
263 samples. The repetition rate was 5 Hz and the count time was 40 s (200 pulses) on the
264 sample and 40 s on the gas blank (background). Concentrations were calibrated using
265 NIST612 with ^{29}Si as the internal standard. Data reduction was performed manually using
266 Microsoft Excel allowing removal of portions of the signal compromised by the occurrence of
267 microcrysts. Full details of the analytical and data reduction methods are given in Tomlinson
268 et al. (2010). Accuracies of ATHO-G and StHs6/80-G MPI-DING glass analyses are
269 typically <5% for most elements and <10% for Nb, Pr, Eu, Gd, and Ta. Reproducibility of
270 StHs6/80-G analyses is <5 RSD% for all trace elements. For consistency with EMPA error
271 reporting, error bars on plots represent the 2 standards deviation of replicate analyses of
272 StHs6/80-G. Relative standard errors (RSE) for LA-ICP-MS tephra samples analyses are
273 typically <2 % for Rb, Sr, Zr, Nb, Ce, Pr; <5% for V, Y, Ba, La, Nd, Sm, Th, U, and <10% for

274 Eu, Dy, Er, Yb, Lu.

275

276 **4.3 Assessment of tephra correlations**

277 Proximal-distal glass correlations are assessed on the basis of (1) visual assessment using
278 a range of major and trace element biplots; (2) multi-element plots in which each tephra is
279 normalised to its proposed proximal equivalent; and (3) statistical distance (D^2) tests. The
280 statistical distance is a measure of the difference between pairs of samples based on both
281 mean and standard deviation (see Perkins et al., 1995). Providing sample pairs are normally
282 distributed, the $D^2_{\text{calculated}}$ value will have a Chi-squared distribution between compositionally
283 identical sample pairs. Where the $D^2_{\text{calculated}}$ value is greater than the D^2_{critical} value then the
284 null hypothesis (that the sample pairs are identical) must be rejected. A $D^2_{\text{calculated}}$ value less
285 than the D^2_{critical} means that the sample pairs cannot be distinguished, however, this does
286 not confirm they are identical. Compositionally identical samples can only be determined if
287 the $D^2 = 0$. In some cases significant statistical distance between tephra units cannot be
288 shown. However, lower D^2 values relative to other sample pairs may indicate greater
289 compositional similarity (Pearce et al., 2008) and provide further confidence in possible
290 correlations as determined by alternative and previously mentioned comparison
291 approaches. Confidence limits (p) values for statistical distance values are defined from the
292 Chi-squared table and depends on the degrees freedom (f). f = the number of elements
293 used to generate the D^2 values. For major elements we used all elements excluding MnO,
294 P₂O₅ and Cl (thus $f = 8$) and for trace element $f = 11$ (Rb, Y, Zr, Nb, La, Ce, Pr, Nd, Sm, Th
295 U). At the 95% confidence limit the D^2_{critical} values for majors and trace elements are 15.5
296 and 19.7 respectively.

297

298 **5. Results**

299 Representative major and trace element analyses of proximal glasses are reported in table
300 3 and the full dataset is available as supplementary data. In presenting the results we will

301 highlight the compositional features that allow the discrimination of different eruptive units
302 thus revealing the diagnostic chemistry that can be used as a fingerprints in proximal-distal
303 tephra correlations.

304

305 **5.1 Proximal glass chemistry**

306 Volcanic glasses produced during explosive eruptions from Ischia are dominantly
307 intermediate silicic (60.6-63.0 wt%) and straddle the phonolite-trachyte boundary (Fig. 2a), a
308 characteristic shared by magmas from the other active Neapolitan volcanoes (Campi Flegrei
309 and Somma-Vesuvius). Proximal Ischia phonolite and trachyte glasses have restricted
310 compositional ranges and show an overall trend of increasing CaO and K₂O and decreasing
311 FeO, Na₂O (Fig. 2b) and total alkalis with increasing SiO₂. They can be distinguished from
312 other Neapolitan magmas by their lower CaO concentrations (<1.80 wt%) (Fig. 2c,d).
313 Proximal Ischia trachyte and phonolite glasses are alkali-rich, with high total alkalis
314 (Na₂O+K₂O = 12.8-14.7 wt%) and high K₂O (>5.8 wt%), therefore Ischia tephra often have
315 K₂O/Na₂O <1 (e.g. Poli et al., 1987) reaching as low as K₂O/Na₂O = 0.7. Mantle-normalised
316 trace element concentrations of proximal Ischia glasses have subduction-related signatures
317 with depletion in the HFSE element relative to the LILE and pronounced depletion in Ba, Sr
318 and Eu in response to the fractionation of K-feldspar, a dominant phenocryst phase in
319 juvenile clasts. Proximal Ischia glasses are highly evolved (Zr/Sr=0.2-600, mean = 128),
320 extending to more highly evolved compositions than Campi Flegrei and Vesuvius tephra),
321 and span a narrow range of Nb/Th (2.3 ± 0.3), partially overlapping with the pre-CI trend
322 (Tomlinson et al., 2012).

323

324 **5.1.1 Pre-MEGT (4 eruptions)**

325 Pre-MEGT glasses are phonolitic to phono-trachytic (Fig. 2a). Using decreasing CaO as a
326 fractionation index reveals a decrease in K₂O and an increase in Na₂O as evolution
327 progresses (Fig. 3a-c). This gives rise to a wide range of alkali compositions in the pre-

328 MEGT tephra (K_2O/Na_2O 0.7 to 1.1). Trace element contents increase sharply with
329 decreasing CaO with Th going from 20 to 80 ppm and Zr from ~300 to ~1100 ppm (Fig. 4a-
330 c). Major and trace element compositional clusters within both the proximal and distal tephra
331 allow two compositional groups to be defined within the pre-MEGT magmatic system

332
333 Pre-MEGT Group 1 glasses have higher incompatible element/Th ratios ($Y/Th = 1.5 \pm 0.5$;
334 $Ta/Th = 0.12 \pm 0.04$ and $Nd/Th = 2.4 \pm 0.8$). On the basis of a compositional gap at Th =
335 30–36 ppm and Zr = 432–550 ppm, they are divided in two sub-groups. Group 1a, with
336 $Th < 30$ ppm, includes the least evolved glasses with high CaO (1.36 ± 0.05 wt%), SiO_2 (62.3
337 ± 0.2 wt%) and K_2O (7.0 ± 0.1 wt%), low FeO (2.5 ± 0.1 wt%) and Na_2O (6.8 ± 0.2 wt%;
338 giving $K_2O/Na_2O = 0.97$ – 1.11) and low incompatible trace element concentrations (Zr < 440
339 ppm, Nb < 57 ppm). Group 1b, with $Th > 36$ ppm, is composed of intermediate glasses with
340 low CaO (1.14 ± 0.08 wt%), intermediate SiO_2 (61.9 ± 0.2 wt%), FeO (2.6 ± 0.1 wt%), K_2O
341 (6.5 ± 0.2 wt%) and Na_2O (7.4 ± 0.2 wt%; giving $K_2O/Na_2O = 0.72$ – 0.95) and moderate
342 incompatible trace element concentrations (Zr = 550–695 ppm, Nb = 95–115 ppm).

343
344 Pre-MEGT Group 2 glasses have lower incompatible element/Th ratios ($Y/Th = 1.2 \pm 0.2$;
345 $Ta/Th = 0.10 \pm 0.01$ and $Nd/Th = 1.8 \pm 0.2$) forming sub-parallel trend on incompatible
346 element bivariate plots. They are the most evolved among the Pre-MEGT rocks, with low
347 CaO (1.05 ± 0.06 wt%) and K_2O (6.1 ± 0.1 wt%), and high FeO (2.8 ± 0.2 wt%), Na_2O ($8.2 \pm$
348 0.2 wt%) and SiO_2 (61.3 ± 0.4 wt%), giving $K_2O/Na_2O = 0.68$ – 0.78 . Incompatible trace
349 element contents are high ($Th \geq 40$ ppm, Zr > 610 ppm, Nb > 80 ppm).

350
351 These compositional groups occur repeatedly in successive Pre-MEGT eruptions as shown
352 in Table 4. Tephra from potentially smaller-volume eruptions (e.g. Sant'Angelo and
353 Porticello tephtras) are composed of glasses from only one of the magma groups, while
354 those from apparently larger-volume eruptions (e.g. the Tisichiello and Olummo tephtras)

355 display glasses from all three compositional groups. The repeated occurrence of these
356 magma groups is problematic for proximal-distal and distal-distal tephra correlations.
357 However, small differences in major and trace element absolute abundances between
358 successive deposits of a given compositional group may be used to fingerprint individual
359 eruptions.

360

361 **5.1.2 MEGT**

362 Glasses in the extracaldera MEGT pumice fall deposit and overlying welded ignimbrite
363 straddle the phono-trachytic boundary and overlap with the least evolved glass
364 compositions of Pre-MEGT group 2. The MEGT glasses extend to less evolved
365 compositions than seen in the Pre-MEGT group 2, with CaO (0.88–1.05 wt%), FeO (2.3–2.7
366 wt%) and Na₂O (7.8–8.2 wt%) and higher K₂O (5.8–6.6 wt%) giving K₂O/Na₂O 0.7–1.4 (Fig.
367 3d-f). Incompatible trace element concentrations span a relatively narrow range (Th 49–58
368 ppm, Zr 679–846 ppm) and lack the more most elevated compositions seen in Pre-MEGT
369 group 2 glasses (Fig. 4d-f).

370

371 Pumice fragments from the lithic breccia at the top of the sequence form a trachytic cluster,
372 that lies beyond the less-evolved end of the Pre-MEGT Sub-group 1a glasses. Relative to
373 Pre-MEGT Sub-group 1a, the MEGT lithic breccia has higher FeO (2.7 ± 0.3 wt%), MgO
374 (0.51 ± 0.11 wt%) and K₂O (7.44 ± 0.5 wt%), higher but overlapping CaO (>1.34 wt%) and
375 lower Na₂O (6.1 ± 0.6 wt%) at constant SiO₂ (62.6 ± 0.4 wt%). The incompatible trace
376 element concentrations are the lowest detected in Ischia glasses at Th <16 ppm; Zr <242
377 ppm, Nb <46 ppm.

378

379 The green and grey pumices of the extracaldera MEGT ignimbrite at Acquamorta (Monte di
380 Procida) are phono-trachytic and overlap with Pre-MEGT group 1 (a and b), spanning a
381 range of CaO (1.04–1.29 wt%), Na₂O and K₂O (K₂O/Na₂O 0.8–1.0). Incompatible element

382 concentrations are variable (Th 24–56 ppm, Zr 367–834 ppm) and fall on a sub-parallel
383 trend of higher Nb and Y for a given Th relative to the studied Pre- and Post-MEGT glasses.
384

385 **5.1.3 Post-MEGT (3 eruptions)**

386 Glasses from Post-MEGT deposits are dominantly trachytic and displaced to lower MgO,
387 FeO and TiO₂ (down to 0.23, 2.1 and 0.42 wt%, respectively; Fig. 3g-l) and incompatible
388 element (Th 13–74 ppm, Zr 211–841 ppm) contents relative to Pre-MEGT and MEGT
389 glasses (Fig. 4g-l). Post-MEGT glasses show a general trend of decreasing CaO and K₂O,
390 and increasing Na₂O, giving rise to a wide range of alkali compositions (K₂O/Na₂O
391 0.86–1.33), incompatible element concentrations increase with decreasing CaO. Major and
392 trace element compositional clusters allow two compositional groups to be defined within
393 the post-MEGT erupted rocks. Post-MEGT Group 1 glasses have higher incompatible
394 element/Th ratios (Y/Th = 1.5 ± 0.2; Ta/Th = 0.13 ± 0.01 and Nd/Th 2.5 ± 0.4), similar, within
395 error, to those of the Pre-MEGT Group 1. They span a wide compositional range from high
396 to intermediate CaO (1.2–1.5 wt%), K₂O (6.6–7.7 wt%) and intermediate to low Na₂O (5.7 to
397 7.1 wt%), giving K₂O/Na₂O values between 0.94 and 1.33. Incompatible element contents
398 are low to moderate (Zr = 210–556 ppm and Th = 13–43 ppm). Post-MEGT Group 2 glasses
399 have lower incompatible element/Th ratios (Y/Th = 1.16 ± 0.05; Ta/Th = 0.10 ± 0.01 and
400 Nd/Th = 1.7 ± 0.1), similar, within the errors, to those of the Pre-MEGT Group 2 glasses.
401 They are the most evolved post-MEGT rocks, with low CaO (0.1–1.3 wt%), K₂O (6.4–6.6
402 wt%) and low Na₂O (7.0–7.5 wt%), giving K₂O/Na₂O 0.86–0.93, and moderate incompatible
403 element contents (Zr 505–630 ppm and Th 35–47 ppm).

404

405 In the studied proximal Post-MEGT sequence, each compositional group is observed only in
406 the deposits of one single eruption (Table 5), however, comparison of our glass data with
407 whole rock data for the same tephra, at different field localities (Civetta et al., 1991), reveal
408 that the Post-MEGT Pietre Rosse and Agnone Tuffs are bimodal in composition displaying

409 both compositional groups. This, coupled with fact that some post-MEGT Ischia tephra
410 layers detected in the distal LGdM record are bimodal, justifies our definition of
411 compositional groups for this period of the Ischia magmatic system. Whilst the Schiappone
412 Tephra and Agnone Tuff both belong to the same Post-MEGT compositional group, they
413 can be easily distinguished as the Agnone Tuff glasses are more enriched in their
414 incompatible trace element concentrations, whilst the Schiappone Tephra glasses have
415 higher K_2O/Na_2O ratios (Fig. 3). There is some overlap between Schiappone Tephra and
416 the MEGT lag Breccia, however, the Schiappone tephra glasses can be distinguished by
417 the absence of the higher MgO concentrations.

418

419 **6. DISCUSSION**

420 In this section, we compare the data on proximal deposits presented above to new major
421 and trace element data for selected Ischia tephra layers from the distal LGdM archive
422 (Table 6), in order to better constrain the timing and frequency of eruptions at Ischia. Ages
423 presented for each LGdM tephra are given as calendar ages BP (1950) following the LGdM
424 varve and sedimentation rate chronology of Brauer et al. (2007). Where applicable, other
425 distally recognised tephra layers from other locations are also discussed. The distinctive
426 and prevalent MEGT tephra is used to divide the LGdM stratigraphy into Pre-MEGT and
427 Post-MEGT periods and so is discussed first.

428

429 **6.1 MEGT**

430 **6.1.1 MEGT LGdM tephra correlations**

431 LGdM tephra TM-19 (60,060 varve years BP) is the thickest layer, and at a trace element
432 level is the most heterogeneous Ischia tephra layer recognised in the LGdM stratigraphic
433 sequence. The TM-19 layer comprises a 2 cm thick, coarse-grained ash fall layer overlain
434 by 30 cm of co-ignimbrite ash with minor sediment. Glass shards in the TM-19 layer are
435 heterogeneous and broadly overlap all three Pre-MEGT groups at a major, minor and trace

436 element level (Fig. 3-4). TM-19 tephra plotting in the Pre-MEGT Group 2 field match the
437 proximal MEGT extra-caldera fall and overlying welded ignimbrite. Both the proximal MEGT
438 fall and TM-19 tephra are restricted in terms of their overall levels of incompatible trace
439 element enrichment and do not extend to the higher concentrations detected in the Pre-
440 MEGT Group 2 rocks Sant'Angelo tephra (flow and lag breccia), Olummo Tephra (lower fall)
441 and Tisichiello Tephra (upper fall). A second cluster of TM-19 glasses fall in the Pre-MEGT
442 group 1 a and b field, but are displaced to higher concentrations of Nd, Sm, Ce and Y for a
443 given Th (Fig. 5), relative to the Pre-MEGT Group 2 and match the extracaldera MEGT
444 deposits from Acquamorta (Monte di Procida). TM-19 also has shards that match the
445 composition of the least evolved MEGT glass population from the lithic breccia at the top of
446 the extracaldera proximal sequence (Fig. 5). In summary the MEGT tephra investigated
447 satisfies more of the compositional variation observed in heterogeneous TM-19 than any of
448 the stratigraphically older or younger eruptive units, thus providing us with a strong
449 correlation. This supports a distal-proximal correlation and re-affirms the interpretation of
450 Wulf et al. (2004). Crucially, the stratigraphic integrity of the TM-19 tephra layer within the
451 varved sediments of LGdM indicates that this compositional heterogeneity is diagnostic of
452 the MEGT eruption.

453

454 **6.1.2 Other distal MEGT equivalents**

455 Other Mediterranean tephra layers that have been stratigraphically associated with early
456 MIS 3 and attributed to explosive activity on Ischia have been re-investigated. These
457 tephra include the southerly dispersed Ionian Sea Y-7 tephra (M25/4-11) and the 'Ischia
458 tephra' layer on Stromboli (ITS) both of which were previously linked to the Sant'Angelo
459 tephra (Keller et al., 1978; Kraml 1997; Lucchi et al., 2008). We have also investigated a
460 marine cryptotephra PRAD 1870 from the Adriatic sea east of Ischia, which has been linked
461 to MEGT (Bourne et al., 2010). Y-7, ITS and PRAD1870 show near identical trace element
462 compositions and heterogeneity to TM-19 and to that of the proximal MEGT tephra

463 investigated (Fig. 5). Furthermore, glasses from the tephra MD 28 (southern Tyrrhenian
464 Sea) appear to show similar heterogeneity consistent with the other distal MEGT
465 equivalents (Fig. 5).

466

467 The earlier correlations of the southerly-dispersed Ionian Sea Y-7 (Keller et al., 1978; Kraml
468 1997) and ITS (Kraml 1997; Lucchi et al., 2008) to the Sant'Angelo Tephra are inconsistent
469 with the glass data presented here. Only the most evolved components of these two distal
470 tephra correspond to Sant'Angelo Tephra Pre-MEGT group 2 glass chemistries and this is
471 equally satisfied by MEGT Plinian fall compositions. The Sant'Angelo Tephra does not
472 match the full geochemical range observed in the Y-7, as it lacks the least evolved Pre-
473 MEGT Group 1 compositions with $K_2O > Na_2O$ and also the intermediate glass compositions
474 with higher Nd and Y for a given Th – both of which are found in the MEGT and present in
475 the TM-19, Y-7 and ITS tephra layers (Fig. 5).

476

477 Other Tyrrhenian Sea ash layers deposited in early MIS 3 sediments showing high Na_2O (>
478 6.wt %) and low CaO content relative to other Campanian volcanic sources have been
479 attributed to the explosive activity of Ischia (Paterne et al., 1986; 1988; Calanchi et al.,
480 1994). The marine layer C-17, recognised by Paterne et al. (1986), was correlated to the
481 caldera-forming MEGT eruption. The stratigraphically lower, thicker and more widespread
482 C-18 tephra layer, was later tentatively correlated with the Ionian Sea Y-7 layer (Paterne et
483 al., 1988; Calanchi et al., 1994), but remained proximally undefined on Ischia (Paterne et
484 al., 1986; 1988; Calanchi et al., 1994). Whilst major data reveals Ischia as a proximal
485 source, data are not directly comparable to proximal glasses presented herein owing to very
486 different analytical parameters (i.e., SEM [Major elements] and neutron activation [Trace
487 elements]). Bulk REE element analyses of glass separates are presented in Paterne et al.
488 (1986). Remembering that bulk glass analyses homogenises any compositional variation,
489 some observations can be made. The thicker, more widespread, C-18 shows significantly

490 higher levels of incompatible trace element enrichment (i.e., Ce 222 ppm; Nd 73 ppm)
491 relative to the C-17 tephra (i.e., Ce 157 ppm; Nd 48 ppm). C-18 concentrations appear to
492 represent an average composition of the distal MEGT equivalents (TM-19, Y-7, ITS and
493 PRAD 1870), whilst the C-17 is less enriched than the distal MEGT equivalents, suggesting
494 that former is a better a correlative of MEGT/TM-19. The precisely defined geochemical
495 correlations linking the Y-7 (Ionian Sea), PRAD-1870 (Adriatic Sea) and the ITS (Southern
496 Tyrrhenian Sea) to the MEGT eruption reveal this to be one of the most widespread late
497 Quaternary markers in the central Mediterranean region (Fig. 6) This is particularly
498 important given its close stratigraphic association with the onset of MIS 3 and its potential to
499 help asses spatial leads and lags in climate archives.

500

501 **6.1.3 Volume and dispersal of MEGT tephra**

502 The locations and thicknesses (where available) of distal MEGT tephra layers are shown in
503 figure 6 and summarized in table 7. Ash produced during the MEGT eruption is confirmed
504 as far as 540 km south-southeast of Ischia where it is recorded as the 4 cm thick Y-7 layer
505 of the Ionian Sea (M25/4-11). This defines the major dispersal axis for this eruption. On the
506 same axis, there are thicknesses of 20 cm in a southern Tyrrhenian Sea core (C-18,
507 KET8003; Paterne et al., 1986) and 17 cm on Island of Stromboli (ITS). To the east, the
508 MEGT tephra is 32 and 10 cm thick at LGdM and San Gregorio Magno, respectively, and is
509 recorded as cryptotephra layers in central (PRAD 1870) and southern Adriatic cores
510 (SA03-03; Bourne 2012). We have used these sites to make a preliminary estimate of the
511 25 and 4 cm isopach curves for MEGT tephra and envisage their dispersal axes. The 4 cm
512 isopach curve has the same axis and ellipticity as the 25 cm isopach, and passes through
513 the Ionian Sea core site (Fig. 6).

514

515 We have used the isopach curves of figure 6 to provide a preliminary estimate of the volume
516 of MEGT tephra deposited by particle fallout. It should be noted that this is a first order

517 estimate, both because the proximal volume is poorly constrained due to poor exposure on
518 Ischia and because it is often not possible to distinguish between Plinian and co-ignimbrite
519 fall in distal locations. The maximum thickness of MEGT fall deposits is 820 cm at Cavone
520 dei Camaldoli on the southern side of Ischia (Brown et al., 2008). Assuming that the 25 and
521 4 cm isopach curves record deposition of tephra by fallout, then the MEGT tephra fall has a
522 volume of $\sim 40 \text{ km}^3$ using the Log Thickness vs. Square Root of the Area (Log T vs. \sqrt{A})
523 method of Pyle et al. (1989), modified by Fierstein and Nathenson (1992). When corrected
524 for the lower density of fall deposits, this is in line with the $\sim 15 \text{ km}^3$ estimate of total erupted
525 magma determined from the size of the caldera (Brown et al., 2008).

526

527 **6.1.4 Chronological constraints on the MEGT**

528 The age of the MEGT eruption was determined on proximal rocks by K/Ar method at about
529 52 to 58 ka (Gillot et al. 1982). Distal equivalents of the MEGT have been directly dated by
530 $^{40}\text{Ar}/^{39}\text{Ar}$, including the ITS layer dated at $56 \pm 4 \text{ ka } ^{40}\text{Ar}/^{39}\text{Ar}$ (Kraml 1997) and the LGdM
531 TM-19 layer dated at $55 \pm 2 \text{ ka}$ (Watts et al., 1996). These proximal and distal ages are in
532 good agreement, and the high-precision age of $55 \pm 2 \text{ ka}$ should be the preferred
533 chronological constraint for the MEGT eruption and other distal equivalents. The $^{40}\text{Ar}/^{39}\text{Ar}$
534 age of the MEGT/TM-19 ash layer suggests that the LGdM calendar age determined for
535 TM-19 (60,040 calendar yr BP) is an overestimate, indeed Wulf et al. (2012) recognised that
536 section 5 (37,000-90,000 calendar yrs BP) in the LGdM record presents ca. 8%
537 overestimate in calendar ages BP.

538

539 **6.2 Proximal-LGdM tephra correlations**

540 **6.2.1 Pre-MEGT LGdM tephra correlations**

541 **6.2.1.1 TM-24-3b (104,020 varve yrs BP) and TM-23-20a (99.350 varve yrs BP)**

542 These two tephras have glass compositions overlap with Pre-MEGT Group 2 glasses but
543 extend to lower CaO ($1.00 \pm 0.04 \text{ wt\%}$) (Fig. 7a) and Na₂O ($7.8 \pm 0.3 \text{ wt\%}$), and higher SiO₂

544 (61.7 ± 0.5 wt%) contents. They have high incompatible element concentrations with (Fig.8
545 c,d). The glasses are displaced to lower ratios of HFSE to Th (i.e., Y/Th = 1.03 ± 0.05)
546 relative to Pre-MEGT Group 2, and consequently form a new sub-parallel Pre-MEGT Group
547 3 trend (Fig, 7c-d) that is not known from the proximal stratigraphy. The compositional
548 differences between TM-24-3b and TM-23-20a preclude correlations with the proximal pre-
549 MEGT units studied here, disproving the proposed correlation between TM-24-3b and
550 Sant'Angelo Tephra (Wulf et al., 2012). Thus the age of TM-24-3b should not be imported
551 into the proximal stratigraphy.

552

553 6.2.1.2 TM-21-2a (80,990 varve yrs BP)

554 This layer, consistent with the Pre-MEGT Group 1a, extensively overlaps with the main
555 Tisichiello glass population (Fig. 7), and has low statistical distance values ($D^2_{\text{majors}} = 0.58$
556 and $D^2_{\text{traces}} = 1.20$) on the basis of which a correlation cannot be excluded at 95%
557 confidence limit. Figure 8c shows the chemical data of TM-21-2a tephra normalised to the
558 average content of the Pre-MEGT Group 1a Tisichiello Tephra samples (OIS 0309 and OIS
559 0311). Whilst these samples are less evolved than the rest of the Tisichello tephra they
560 represent the first erupted and coarsest pumice fall deposits of the Tisichello eruption and
561 so may be more widely dispersed than the more evolved later products (OIS 0314 and OIS
562 0315). The LGdM tephra typically lies within 10% of the proximal Pre-MEGT sub-group 1a
563 tephra for all major and trace elements. Therefore, we tentatively suggest a correlation
564 between TM-21-2a and Tisichiello Tephra.

565

566 6.2.1.3 TM-20-5 (72,940 varve yrs BP)

567 This layer has Pre-MEGT Group 2 glass composition. Of the studied proximal glasses, TM-
568 20-5 is most similar to that of the Olummo Tephra ($D^2_{\text{majors}} = 0.59$ and $D^2_{\text{traces}} = 1.51$),
569 however small but significant systematic differences exist. TM-20-5 extends to lower CaO
570 and MgO contents and its average HFSE concentrations that are consistently 5% lower

571 than Olummo values (Fig. 8b). Therefore, we do not correlate TM-20-5 with the proximal
572 Olummo formation on Ischia. In fact, a TM-20-5-Olummo correlation would be inconsistent
573 with the proposed link between the older LGdM TM-21-2a tephra and the overlying
574 Tisichiello Tephra.

575

576 *6.2.1.4 TM-20 (61,370 varve yrs BP), TM-20-1b (64,140 varve years BP) and TM-20-1c*
577 *(64,470 varve yrs BP).*

578 These three tephra layers have very similar Pre-MEGT Group 1b glass compositions (CaO
579 <1.2 wt.% and MgO < 0.4 wt. % and exclusively Na₂O > K₂O) with limited compositional
580 variation and thus are potential distal equivalents of the Porticello Tephra. A fourth LGdM
581 layer, TM-20-1a (64.0 ka) was not analysed. The three studied distal tephras show
582 extensive overlap with Porticello Tephra on all major and trace element biplots (Fig. 7).
583 When compared to Porticello Tephra, calculated D² values are close to 1 for all three LGdM
584 tephras (TM-20 D²_{major} = 0.87, D²_{trace} = 1.16; TM-20-1b D²_{major} = 1.06, D²_{trace} = 0.46; TM-20-
585 1c D²_{major} = 0.81, D²_{trace} = 0.87), significantly below D²_{critical}. Figure 8e-f shows that all three
586 distal tephra generally lie within 10% of Porticello Tephra for all major and trace elements
587 and fall within the envelope defined by the proximal Porticello Tephra glasses. However,
588 this plot shows that, although concentrations of Rb, Zr, Nb, Ta, Th and U in TM-20 are
589 within the concentration range defined by the proximal Porticello tephra, average
590 concentrations of these elements are offset to 5% higher values. Therefore, we favour a
591 correlation with TM-20-1b and/or TM-20-1c tephra. This correlation raises the possibility that
592 the Porticello Tephra includes the deposits of more than one, but perhaps two closely
593 spaced eruptions.

594

595 Previous distal-proximal correlations have linked tephra TM-20 with the Sant'Angelo Tephra
596 of Ischia (Wulf et al., 2004). The Sant'Angelo Tephra deposits have Pre-MEGT Group 2
597 compositions (Table 4), in contrast to TM-20, TM-20-1b and TM-20-1c which all have a Pre-

598 MEGT Group 1a compositions. Therefore glass data presented herein does not support the
599 previous correlations of TM-20 to the Sant'Angelo Tephra.

600

601 Previous distal-distal tephra correlations have linked LGdM tephra TM-20 with the distal
602 marine tephra Y-7 (Wulf et al., 2004). Wulf et al., (2006) later proposed a correlation
603 between LGdM tephtras TM-20-1b and TM-20-1c and the Y-7 marine tephra. However,
604 these correlations are not supported by our major and trace element glass data. The Y-
605 7/MEGT tephra has Pre-MEGT Group 1a, Group 1b and Group 2 chemistries with both
606 $\text{Na}_2\text{O} > \text{K}_2\text{O}$ and $\text{K}_2\text{O} > \text{Na}_2\text{O}$ and a wide ranging trace element concentrations (Zr 225-803
607 ppm, and Th 16-53 ppm), thus inconsistent with the TM-20, TM-20-1b and TM-20-1c
608 glasses. Munno and Petrosino (2007) correlated the S-15 tephra recorded in the San
609 Gregorio basin sequence to TM-20. However, as the S-15 tephra has $\text{K}_2\text{O} > \text{Na}_2\text{O}$, the
610 correlation must be rejected on these grounds.

611

612 **6.2.2 Post-MEGT LGdM tephra correlations**

613 *6.2.2.1 TM-18-17a (55,620 varve yrs BP)*

614 This tephra layer is compositionally variable, with 1.3-1.8 wt% CaO, 61.7-62.8 wt% SiO_2
615 and $\text{K}_2\text{O}/\text{Na}_2\text{O}$ ratios of 1.1-1.6 and low concentrations of incompatible trace elements (Th
616 13-24 ppm, Zr 204-360 ppm) falling into Post-MEGT Group 1. TM-18-17a shows a complete
617 overlap with glasses from the Schiappone Tephra (Fig. 9a-d). The dominant population of
618 LGdM tephra lies within 5% of the average composition of the least evolved glass in the
619 Schiappone pumice fall deposit (SC-MEGT 0313) and ignimbrite (SC-MEGT 0315l) deposits
620 of the Schiappone Tephra. A subordinate number of LGdM clasts extend to the less evolved
621 compositions, and are within the envelope defined by the darker clasts in the PDC deposits
622 (SC-MEGT 0315g) of the Schiappone Tephra (Fig. 9e). Therefore, we suggest that the
623 Schiappone Tephra is the proximal equivalent of TM-18-17a layer.

624

625 Paterne et al. (1986) correlated the C-16 Tyrrhenian Sea tephra with the Upper Scarrupata
626 di Barano Formation (Vezzoli 1988) on Ischia, these deposits have been subsequently
627 included into the Schiappone Tephra (Brown et al., 2008). The following lines of evidence
628 might support the existing correlation between Schiappone/TM-18-17a and C-16. C-16
629 chemical data presented by Paterne et al. (1986, 1988) from multiple cores show highly
630 variable glass compositions with exclusively $K_2O > Na_2O$, consistent with those of the
631 Schiappone Tephra. Concentrations of CaO are >1.3 wt% with a maximum of 2.5 wt%. This
632 range is comparable to that displayed by proximal light and dark juvenile fragments of the
633 Schiappone Tephra. Furthermore, bulk glass REE concentrations of C-16 overlap with the
634 most evolved Schiappone glasses presented herein. Tyrrhenian Sea core tephra layer C-
635 17, linked to MEGT by Paterne et al. (1986, 1988), is also a potential equivalent of
636 Schiappone/TM-18-17a. The C-17 compositional data (Paterne et al. 1986) extend to higher
637 (~ 1) K_2O/Na_2O values and lower (0.67-0.91 wt%) CaO content with overlapping REE
638 concentrations. While a correlation between Schiappone/TM-18-17a and C-17 cannot be
639 excluded, yet a C-16 tephra is a more convincing candidate on the basis of the available
640 data.

641

642 6.2.2.2 TM-18-14a (50,260 varve yrs BP)

643 This tephra layer is compositionally variable, with concentrations of CaO ranging from 1.2 to
644 1.7 wt%, and SiO_2 from 61.7 to 62.9 wt%, and K_2O/Na_2O values between 0.9 and 1.5, and
645 low to moderate incompatible trace element contents (Th 10.5-43.5 ppm, Zr 166-605 ppm).
646 TM-18-14a is bimodal, the first population has CaO 1.31 ± 0.16 wt% and Th >35 ppm lie on
647 the Post-MEGT Group 2 trend defined by the proximal deposits of the Pietre Rosse Tuff
648 (Fig. 9a-d). The trace element composition of this TM-18-14a population is a good match for
649 Pietre Rosse Tuff, falling within 10% of the average Pietre Rosse trace element composition
650 ($D^2_{\text{trace}} = 0.60$). The major element composition of TM-18-14a is also a reasonable match
651 ($D^2_{\text{major}} = 1.77$), however the CaO content is displaced to overlapping but higher CaO than

652 Pietre Rosse glasses (Fig. 8f). The second TM-18-14a population has Th<35 ppm fall on
653 the Post-MEGT Group 1 trend and extend to less evolved compositions (CaO 1.3-1.7 wt%,
654 Th 10-33 ppm, Zr 166-490 ppm). Whole-rock compositions comparable to this less evolved
655 TM-18-14a population are reported for Pietre Rosse Tuff by Civetta et al. (1991). We
656 suggest a correlation between TM-18-14a and Pietre Rosse given the good age and trace
657 element match, while noting a minor offset in major element composition.

658

659 6.2.2.3 TM-18-9e (41,700 varve yrs BP)

660 This tephra layer forms a cluster on major and trace element biplots with CaO = 1.28 ± 0.16
661 wt%, SiO₂ = 62.9 ± 0.5 wt% and K₂O/Na₂O = 1.0 ± 0.1 . Incompatible element contents are
662 moderate (Th = 36 ± 2 ppm, Zr = 506 ± 37 ppm) and lie on post-MEGT trend 1 with high
663 incompatible element/Th. TM-18-9e glasses overlap with the proximal Agnone Tuff on major
664 and trace element biplots. The LGdM tephra TM-18-9e is offset to lower CaO (up to 30%)
665 and LREE-MREE (up to 20%) contents relative to Agnone Tuff. This is reflected in the
666 higher statistical distance values of $D^2_{\text{major}} = 2.03$ and $D^2_{\text{trace}} = 9.57$. Therefore, while we
667 cannot exclude a correlation between TM-18-9e and Agnone Tuff at 95% confidence, we do
668 not consider such a correlation to be likely.

669

670 6.2.2.4 TM-18-9a (41,420 varve yrs BP)

671 This tephra layer spans a narrow compositional range, with CaO 1.43 ± 0.07 wt% and
672 K₂O/Na₂O = 1.1 ± 0.1 . TM-18-9a is a moderately evolved (Zr 335-454 ppm; Th 22-32 ppm)
673 Post-MEGT group 1 tephra that sits in the gap between Agnone and Pietre Rosse (Fig. 9a-
674 d) and does not correlate with any of the proximal units studied here.

675

676 6.2.2.5 TM-17-1c (34,980 varve yrs BP)

677 This tephra layer has two compositional modes. The dominant population has low CaO
678 (1.18 ± 0.05 wt%) and MgO (0.24 ± 0.02 wt%), high K₂O/Na₂O (0.89 ± 0.03) and moderate

679 incompatible element concentrations (Th = 43 ± 2 ppm; Zr = 582 ± 19 ppm and Nb = 91 ± 2
680 ppm) that lie in post-MEGT trend 2. This dominant TM-17-1c cluster overlaps extensively
681 with the proximal Pietre Rosse glass data ($D_{\text{major}}^2 = 1.49$ and $D_{\text{trace}}^2 = 0.08$). A second glass
682 population is similar in composition to the low-Th whole-rock composition reported for Pietre
683 Rosse Tuff by Civetta et al. (1991). Whilst chemically tephra TM-17-1c is also a good match
684 for Pietre Rosse, chronologically it is probably too young to represent the 46 ka (K-Ar) Pietre
685 Rosse (Civetta et al., 1991) thus we prefer a correlation with TM-18-14a. This emphasises
686 the importance of integrating chemical, stratigraphic and chronological information when
687 establishing proximal-distal correlations.

688

689 **6.2.3 Age constraints from proximal-LGdM tephra correlations**

690

691 In total, we define five proximal-LGdM tephra correlations on the basis of robust major and
692 trace element glass data: TM-21-2a/Tisichiello, TM-20-1b,c/Porticello, TM-19/MEGT, TM-
693 18-17a/Schiappone and TM-18-14a/Pietre Rosse (Fig. 10). These correlations allow ages
694 from the varved LGdM record to be imported into the proximal stratigraphy of Ischia. The
695 advantage of using the continuous chronostratigraphic record of LGdM is that it allows the
696 relative timing of closely-spaced eruptions to be resolved with a high degree of precision.
697 The absolute ages are overestimated by ca. 8% in the relevant section of the LGdM core
698 (section 5, 37,000-90,000 calendar yrs BP) as a result of incremental counting errors (Wulf
699 et al., 2012). However, the TM-19 layer has been directly dated by laser $^{40}\text{Ar}/^{39}\text{Ar}$ of
700 sanidine, giving an age of 55 ± 2 ka (Watts et al., 1996) for the MEGT. Therefore, we use
701 TM-19 as a chronological anchor for this portion of the LGdM record and then count varve
702 years from this independently dated tephra to generate more accurate ages for the
703 surrounding tephra layers. This works well for the Post-MEGT portion of the core giving
704 counting errors of $\pm 5\%$, but less well in the Pre-MEGT section where the core is not well
705 laminated and counting errors are closer to $\pm 10\%$.

706

707 Applying the differential dating method to the Pre-MEGT, the correlation between Tisichiello
708 and TM-21-2a (80,990 varve years BP) implies an age of 76 ± 3 ka for the Tisichiello
709 eruption. Proximally, the Tisichiello deposits overlie the 74 ka Parata lava (Poli et al., 1987)
710 from which they are separated by Mago and Olummo tephra deposits. The Porticello
711 eruption is correlated with LGdM tephras TM-20-1b (64,140 varve years BP) and/or TM-20-
712 1c (64,470 varve yrs BP). The varve interval between TM-19 and TM-20-1c/TM-20-1b is
713 4080 and 3990 calendar years, giving a differential age of $59 \text{ ka} \pm 2 \text{ ka}$ for the Porticello
714 tephra.

715

716 In the Post-MEGT time period, the age of TM-18-17a (55,620 varve yrs BP) gives an
717 differential age of 50.6 ± 2.0 ka for the voluminous Schiappone Tephra eruption. This is
718 consistent with the proximal K/Ar ages determined for the Schiappone Tephra, which are
719 generally 5 ka younger than the MEGT (Vezzoli, 1988; Brown et al., 2008). The Pietre
720 Rosse tephra is dated at 45 ± 2 ka by differential dating of LGdM tephra TM-18-14a (50,260
721 varve yrs BP). This is comparable to the K-Ar age of 46 ka reported by Civetta et al. (1991).

722

723 **7. Conclusions**

724 The largest known eruption of Ischia was the $\sim 40 \text{ km}^3$, 55 ka MEGT, based on revised
725 proximal-distal tephra correlations we can extend the main south-south east dispersal to at
726 least 540 km. Distal equivalents of the MEGT occur in the Ionian (Y-7), Tyrrhenian (C-18),
727 and Adriatic (PRAD 1870) seas as well as at several locations in southern Italy. Thus, the
728 MEGT is one of the most widely dispersed late Quaternary tephras from the Campanian
729 region.

730

731 Tephra layers in the varved Lago Grande di Monticchio (LGdM) provide a valuable temporal
732 record of Ischia magmatism. The MEGT is correlated with TM-19 in LGdM, which has been

733 directly dated at 55 ± 2 ka (Watts et al., 1996). Differential dating, achieved by varve
734 counting above and below the TM-19 tephra layer gives ages for LGdM tephra layers TM-
735 21-2a (76 ± 3 ka), TM-20-1b,c (62-57 ka), TM-18-17a (50.6 ± 2.0 ka) and TM-18-14a (45
736 ± 2 ka), which are correlated with Tisichiello, Porticello, Schiappone and Pietre Rosse,
737 respectively. Previously suggested correlations between the Sant'Angelo tephra and TM-24-
738 3b are not supported by our glass chemical data.

739

740 Proximal and distal LGdM tephra record a series of geochemical changes during the
741 magmatic history of Ischia. Tephra compositions from the pre-MEGT (Sant'Angelo tephra to
742 Porticello Tephra) period comprise three compositional groups that occur repeatedly in
743 successive eruptions. Tephra from smaller eruptions (e.g. Sant'Angelo tephra and
744 Porticello) contain just one group, while larger eruptions (e.g. Tisichiello and Olummo)
745 record all three groups. Older tephra layers from LGdM (TM-24-3b and TM-23-20a) define a
746 more evolved pre-MEGT compositional group not detected in the proximal rocks. Post-
747 MEGT tephra (<55 ka) record a step to lower FeO and TiO₂ and form compositional groups
748 that overlap with the pre-MEGT but are displaced to lower incompatible element contents.
749 The repeated occurrence of glass compositions means that it is difficult to perform proximal-
750 distal and distal-distal correlations for Ischia tephra without high quality major and trace
751 glass data. This is particularly true for the smaller eruptions that typically show less
752 compositionally variability.

753

754 *Acknowledgements: This work is funded by the NERC RESET Consortium (NE/E015905/1). This is*
755 *paper number ROX/0036. PA thanks Mauro Rosi for field guidance when sampling the Ischia tephra*
756 *on Stromboli, Mark Hardiman is thanked for providing data for one LGdM tephra layer.*

757

758 | REFERENCES

759 Allen, Judy R M; Brandt, Ute; Brauer, Achim; Huntley, Brian; Keller, Jörg; Kraml, Michael;

760 Mackensen, Andreas; Mingram, Jens; Negendank, Jörg F W; Nowaczyk, Norbert R;
761 Watts, William A; Wulf, Sabine; Zolitschka, Bernd; Hubberten, Hans-Wolfgang;
762 Oberhänsli, Hedi (1999): Rapid environmental changes in southern Europe during
763 the last glacial period. *Nature*, 400 (6746), 740-743

764 Bourne A. J., Lowe J. J., Trincardi F., Asioli A., Blockley S. P. E., Wulf S., Matthews I. P.,
765 Piva A. and Vigliotti L. (2010) Distal tephra record for the last ca 105,000 years from
766 core PRAD 1–2 in the central Adriatic Sea: implications for marine
767 tephrostratigraphy. *Quaternary Sci. Rev.* 29(23–24), 3079–3094.

768 Brauer, A., Allen, J.R.M., Mingram, J., Dulski, P., Wulf, S. and Huntley, B. (2007) Evidence
769 for last interglacial chronology and environmental change from Southern Europe.
770 *Proc. Natl. Acad. Sci. U. S. A.*, 104 (2) 450-455.

771 Brown RJ, Orsi G, de Vita S (2008). New insights into Late Pleistocene explosive volcanic
772 activity and caldera formation on Ischia (southern Italy). *Bulletin of Volcanology*
773 70:583–603.

774 Brown RJ and Branney MJ, (2013) Internal flow variations and diachronous sedimentation
775 within extensive, sustained, density-stratified pyroclastic density currents flowing
776 down gentle slopes, as revealed by the internal architectures of ignimbrites on
777 Tenerife. *Bulletin of Volcanology* 75, 727

778 Brown, R.J, Civetta, L., Arienzo, I., D’Antonio, Moretti, R., Orsi, G., Tomlinson, E.L., Albert,
779 P.G., Menzies, M.A.. (2014) Geochemical and isotopic insights into the assembly,
780 evolution and disruption of a magmatic plumbing system before and after a
781 cataclysmic caldera collapse at Ischia volcano (Italy). *Contributions to Mineralogy*
782 and Petrology, [168, 1035 DOI 10.1007/s00410-014-10-](https://doi.org/10.1007/s00410-014-10-168-1035)
783 Bruno P, de Alteriis G, Florio G (2002) The western undersea section of the Ischia volcanic
784 complex (Italy, Tyrrhenian Sea) inferred by marine geophysical data. *Geophys Res*
785 *Let* 29: Art. No. 1343
786

787 Buchner G, Italiano A, Vita-Finzi C (1996) Recent uplift of Ischia, Southern Italy. In: Jones,
788 W. J., Jones, A. P., and Neuberg, J. (Eds) Volcano instability on the Earth and other
789 planets, Geol Soc Spec Pub 110: 249–252

790 Calanchi N, Gasparotto G and Romagnoli C (1994) Glass chemistry in volcanoclastic
791 sediments of ODP Leg 107, Site 650, sedimentary sequence: provenance and
792 chronological implications. *J. Volcanol. Geotherm. Res.*, 60, 59-85.

793 Cassidy, M., Watt, S. F.L., Palmer, M.R., Trofimovs, J., Symons, W., Maclachlan, S.E.,
794 Stinton, A.J (in press). Construction of volcanic records from marine sediment cores:
795 a review and case study (Montserrat, West Indies). *Earth Science Reviews*.

796 Civetta L, Gallo G, Orsi G (1991) Sr- and Nd-isotope and trace element constraints on the
797 chemical evolution of Ischia (Italy) in the last 55 ka. *J Volcanol Geotherm Res* 46:
798 213–230

799 Crisci GM, de Francesco AM, Mazzuoli R, Poli G, Stanzione D (1989) Geochemistry of the
800 recent volcanics of Ischia Island, Italy: evidences of crystallization and magma
801 mixing. *Chem Geol* 78: 15–33

802 D'Antonio M., Tonarini S., Arienzo I., Civetta L., Dallai L., Moretti R., Orsi G., Andria M.,
803 Trecalli A. - 2013 - Mantle and crustal processes in the magmatism of the Campania
804 region: inferences from mineralogy, geochemistry, and Sr-Nd-O isotopes of young
805 hybrid volcanics of the Ischia island (South Italy). *Contr. Miner. Petrol.*, 165:1173-
806 1194, doi:10.1007/s00410-013-0853-x.

807 de Vita S, Sansivero F, Orsi G, Marotta E (2006) Cyclical slope instability and volcanism
808 related to volcano-tectonism in resurgent calderas: the Ischia island (Italy) case
809 study. *Engen. Geol.* 86: 148–165

810 Della Seta M., Marotta E., Orsi G., de Vita S., Sansivero F., Fredi P. - 2012 - Slope
811 instability induced by volcano-tectonism as an additional source of hazard in active
812 volcanic areas: the case of Ischia island (Italy): *Bull. Volcanol.*, 74: 79-106,
813 doi:10.1007/s00445-011-0501-0.

814 Di Napoli R., Aiuppa A., Bellomo S., Brusca L., D'Alessandro W., Gagliano Candela E.,
815 Longo M., Pecoraino G., and Valenza M. (2009), A model for Ischia hydrothermal
816 system: Evidences from the chemistry of thermal groundwaters, *J. Volcanol.*
817 *Geotherm. Res.*, 186, 133–159

818 Di Napoli R., Martorana R., Orsi G., Aiuppa A., Camarda M., De Gregorio S., Gagliano
819 Candela E., Luzio D., Messina N., Pecoraino G., Bitetto M., de Vita S., Valenza M. -
820 2011 - Highlights on the structure of hydrothermal systems from an integrated
821 geochemical, geophysical and geological approach: the Ischia Island case study.
822 *Geochem. Geophys. Geosyst.*, 12, Q07017, doi:10.1029/2010GC003476.

823 Forcella F, Gnaccolini M, Vezzoli L (1982) I depositi piroclastici del settore sud-orientale
824 dell'isola d'Ischia (Italia). *Riv It Paleont Strat* 89: 135–170

825 Gillot PY, Chiesa S, Pasquare G, Vezzoli L (1982) < 33 000 yr K/Ar dating of the volcano-
826 tectonic horst of the isle of Ischia, Gulf of Naples. *Nature* 229: 242

827 Hornig-Kjarsgaard, I., Keller, J., Koberski, U., Stadlbauer, E., Francalanci, L. & Lenhart, R.,
828 (1993): The Evolution of Stromboli Volcano.- In: Manetti, P. & Keller J. (Eds): The
829 island of Stromboli: Volcanic history and magmatic evolution. *Acta Vulcanologica*
830 3,21-68.

831 Keller J, Ryan WBF, Ninkovich D, Altherr R (1978) Explosive volcanic activity in the
832 Mediterranean over the past 200,000 yr as recorded in deep-sea sediments. *Geol*
833 *Soc Am Bull* 89: 591–604

834 Keller, J. (1969): Ritrovamenti di tufi alkali-trachitici della Campania nelle Isole Eolie.- *Atti*
835 *Acc. Gioenia Catania, Ser. VII, Vol. I, 1-9.*

836 Keller, J. (1981): Quaternary tephrochronology in the Mediterranean region.- NATO,
837 *Advanced Study Institutes Series, Tephra Studies (S. Self & S. Sparks, Ed.), 227-*
838 *244.*

839 Keller, J. (1994): Tephrochronology in the Ionian deep sea basin. In: Hieke, W., Halbach, P.,
840 Türkay, M. & Weikert, T. Mittelmeer 1993, Cruise No. 25 METEOR-Berichte 94-3,
841 165-167.

842 Keller, J., (1980) The island of Salina. Rendiconti della Società Italiana di Mineralogia e
843 Petrologia. 36, pp 489–524.

844 Kraml M. (1997) Laser-40Ar/39Ar-Datierungen an distalen marinen Tephren des jung-
845 quartären mediterranen Vulkanismus. Ph.D, Albert-Ludwigs-Universität Freiburg.

846 Lourens L.J. (2004) Revised tuning of Ocean Drilling Program Site 964 and KC01B
847 (Mediterranean) and implications for the $\delta^{18}\text{O}$, tephra, calcareous nannofossil, and
848 geomagnetic reversal chronologies of the past 1.1 Myr. *Paleoceanography*, 19(3),
849 DOI: 10.1029/2003PA000997

850 Lowe, J.J., et al., 2007. Age modelling of late Quaternary marine sequences in the Adriatic:
851 towards improved precision and accuracy using volcanic event stratigraphy.
852 *Continental Shelf Research* 27 (3–4), 560–582.

853 Lucchi, F., Tranne, C.A., De Astis, G, Keller, J., Losito, R., Morche, W (2008) Stratigraphy
854 and significance of Brown Tuffs on the Aeolian Islands (southern Italy). *Journal of*
855 *Volcanology and Geothermal Research* 177, 49–70.

856 Morche, W (1988) Tephrochronologie der Aolischen Inseln. PhD Thesis, Albert-Ludwigs-
857 Universität Freiburg, Germany.

858 Moretti R., Arienzo I., Orsi G., Civetta L., D'Antonio M. - 2013 - The deep plumbing system
859 of the Ischia island (southern Italy): a physico-chemical and geodynamic window on
860 the fluid-sustained and CO₂-dominated magmatic source of Campanian volcanoes. *J.*
861 *Petrol.*, 54 (5): 951-984.

862 Munno, R., Petrosino, P (2007) The late Quaternary tephrostratigraphical record of the San
863 Gregorio Magno basin (southern Italy). *Journal of Quaternary Science*. 22. 247-266.

864 Müller W., Shelley M., Miller P. and Broude S. (2009) Initial performance metrics of a new
865 custom-designed ArF excimer LA-ICPMS system coupled to a two-volume laser-

- 866 ablation cell. *J. Anal. Atom. Spectrom.* 24(2), 209–214.
- 867 Negri, A., Capotondi, L. & Keller, J. (1999): Calcareous nannofossils and planctonic
868 foraminifera and oxygen isotopes in the late Quaternary sapropels of the Ionian
869 Sea.- *Marine Geol.* 157, 89-103
- 870 Orsi G, Gallo G, Zanchi A (1991) Simple-shearing block resurgence in caldera depressions.
871 A model from Pantelleria and Ischia. *J Volcanol Geotherm Res* 47: 1–11
- 872 Orsi G, Patella D, Piochi M, Tramacere A (1999) Magnetic modelling of the Phlegraean
873 Volcanic District with extension to the Ponza archipelago, Italy. *J Volcanol Geotherm*
874 *Res* 91: 345–360
- 875 Orsi G, Piochi M, Campajola L, D'Onofrio A, Gialanella L, Terrasi F (1996) 14C
876 geochronological constraints for the volcanic history of the island of Ischia (Italy) over
877 the last 5000 years. *J Volcanol Geotherm Res* 71: 249–257
- 878 Paterne M, Guichard F, Labeyrie J (1988) Explosive activity of the South Italian volcanoes
879 during the past 80,000 years as determined by marine tephrochronology. *J Volcanol*
880 *Geotherm Res* 34: 153–172
- 881 Paterne, M., Guichard, F., Labeyrie, J., Gillot, P. Y. & Duplessy, J. C. (1986) Tyrrhenian Sea
882 tephrochronology of the oxygen isotope record for the past 60,000 years. *Marine*
883 *Geology* 72, 259-285.
- 884 Pearce, N.J.G., Alloway, B.V., Westgate, J.A. 2008. Mid-Pleistocene silicic tephra beds in
885 the Auckland region, New Zealand: Their correlation and origins based on trace
886 element analyses of single glass shards. *Quaternary International.* 178, 16-43.
- 887 Perkins, M.E., Nash, W.P., Brown, F.H., Fleck, R.J., 1995. Fallout tuffs of Trapper Creek,
888 Idaho: a record of Miocene explosive volcanism in the Snake River Plain volcanic
889 province. *Geological Society of America Bulletin* 107 (12), 1484–1506.
- 890 Piochi M, Civetta L, Orsi G (1999) Mingling in the magmatic system of Ischia (Italy) in the
891 past 5 ka. *Min Pet* 66: 227–258

- 892 Piva A, Asioli A, Schneider R, Trincardi F, Andersen N, Colmenero Hidalgo E, Dennielou B,
893 Flores J, Vigliotti L (2008) Climatic cycles as expressed in sediments of the
894 PROMESS1 borehole PRAD1-2, central Adriatic, for the last 370 ka: 1. Integrated
895 stratigraphy - art. no. Q01R01. *Geochemistry Geophysics Geosystems*, 9, DOI:
896 10.1029/2007GC001713
- 897 Poli S, Chiesa S, Gillot P–Y, Gregnanin A, Guichard F (1987) Chemistry versus time in the
898 volcanic complex of Ischia (Gulf of Naples, Italy): evidence of successive magmatic
899 cycles. *Contrib Min Pet* 95: 322–335
- 900 Pyle, DM (1989) The thickness, volume and grainsize of tephra fall deposits. *Bull. Volcanol.*,
901 51, 1-5
- 902 Rosi M, Sbrana A, Vezzoli L (1988) Correlazioni tefrostratigrafiche di alcuni livelli di Ischia,
903 Procida e Campi Flegrei. *Mem Soc Geol It* 41: 1015–1027
- 904 Sbrana A. (2009) Carta geologica d'Ischia, Foglio 464 Ischia (scale 1:10 000 CARG
905 Regione Campania)
- 906 Tamburrino (2008) Mediterranean tephrochronology: new insights from high-resolution
907 analyses of a 200,000 years long composite sedimentary log. Ph.D thesis, Università
908 Degli Studi di Napoli “Frederico II”.
- 909 Tibaldi A, Vezzoli L (1998) The space problem of caldera resurgence: an example from
910 Ischia Island, Italy. *Geol Rund* 87: 53–66
- 911 Tomlinson E.L, Arienzo, I, Wulf S, Smith V.C, Carandente A, Civetta L, Hardiman M, Lane
912 C.S, Orsi G, Rosi M, Thirlwall M.T, Muller W and Menzies, M.A. (2012) Geochemistry
913 of the Phlegraean Fields (Italy) proximal sources for major Mediterranean tephra:
914 implications for the dispersal of Plinian co-ignimbritic components of explosive
915 eruptions. *Geochim. et Cosmochim. Acta* 93, 102-128
- 916 Tomlinson, E.L., Thordarson, T., Muller, W., Thirlwall, M., Menzies, M.A., 2010. Micro
917 analysis of tephra by LA-ICP-MS — strategies, advantages and limitations assessed
918 using the Thorsmork ignimbrite (Southern Iceland). *Chemical Geology* 279 (3–4), 73–

919 89.

920 Tonarini S., Leeman W. P., Civetta L., D'Antonio M., Ferrara G. and Necco A. (2004) B/Nb
921 and systematics in the Phlegrean Volcanic District (PVD). *J. Volcan. Geoth. Res.*
922 113, 123–139.

923 Vezzoli L (Ed) (1988) *Island of Ischia. Quaderni de La Ricerca Scientifica, Consiglio*
924 *Nazionale delle Ricerca, Rome* 114 pp.133

925 Vezzoli, L., Principe, C., Malfatti, J., Arrighi, S., Tanguy, J-C., Le Goff, M., Modes and times
926 of caldera resurgence: The < 10 ka evolution of Ischia Caldera, Italy, from high-
927 precision archaeomagnetic dating. *J. Volcan. Geoth. Res.* 186, 3-4, 305-319.

928 Watts, W.A., Allen, J.R.M., Huntley, B. (1996) Vegetation history and palaeoclimate of the
929 last glacial period at Lago Grande di Monticchio, southern Italy. *Quaternary Science*
930 *Reviews* 15, 133–153

931 Wulf S, Kraml M, Brauer A, Keller J, Negendank JFW (2004) Tephrochronology of the 100
932 ka lacustrine sediment record of Lago Grande di Monticchio (southern Italy). *Quat Int*
933 122: 7–30

934 Wulf, S., Brauer, A., Mingram, J., Zolitschka, B., Negendank, J.F.W (2006) Distal tephras in
935 the sediments of Monticchio Marr lakes. In: Principe, C (E.d.), *La geologia del Mone*
936 *Vulture. Regione Basilicata- Consiglio Nazionale delle Ricerche* pp 105-122.

937 Wulf, S., Keller, J., Paterne, M., Mingram, J., Lauterbach, S., Opitz, S., Sottit, G., Giaccio,
938 B., Albert, P.G., Satow, C., Tomlinson, E.L., Vicccaro, M., Brauer, A. (2012). The
939 100-133 ka record of Italian explosive volcanism and revised tephrochronology of
940 Lago Grande di Monticchio. *Quaternary Science Reviews*, 58, 104-123.

941 Zembo I, Vignola P, Andò S, Bersezio R and Vezzoli L (2011). Tephrochronological study in
942 the quaternary Val d'Agri intermontane basin (southern Apennines, Italy). *Int. J. Earth*
943 *Sci.*, 100, 173-187

Table captions

Table 1: Summary of proximal Ischia samples studied. Samples used in previous studies: 1 – Civetta et al. (1991); 2 – Brown et al. (2008). K-Ar ages are from *Gillot et al. (1982), $^{40}\text{Ar}/^{39}\text{Ar}$ (Vezzoli (1988) for units previously correlated with the MEGT) and $^{40}\text{Ar}/^{39}\text{Ar}$ (Poli et al. (1987)). Mineral abbreviations: Alk fsp – alkali feldspar, bt – biotite, cpx – clinopyroxene; plag – plagioclase, neph – nepheline.

Table 2: Summary of Lago Grande di Monticchio tephra layers studied. Varve ages are from Brauer et al. (2007). Mineral abbreviations: Alk fsp – alkali feldspar, bt – biotite, cpx – clinopyroxene; plag – plagioclase, ac – acmite, ti – titanite, ap – apatite.

Table 3: Representative major (EMPA) and trace (LA-ICP-MS) element composition of proximal volcanic glass. Major elements are normalized to 100% and the analytical total given. The full dataset is given as online supplementary data.

Table 4: Geochemical groupings of the Pre-MEGT stratigraphy investigated on Ischia.. The sampled units follow the stratigraphy outlined in Brown et al. (2008; 2014).

Table 5: Geochemical groupings of the Post-MEGT stratigraphy investigated on Ischia. The sampled stratigraphic units follow the descriptions of Brown et al. (2008; 2014) and Civetta et al. (1991).

Table 6: Representative major (EMPA) and trace (LA-ICP-MS) element composition of Lago Grande di Monticchio tephra units. Major elements are normalized to 100% and the analytical total given. The full dataset is given as online supplementary data.

Table 7: Distal occurrences of MEGT tephra used in volume calculation.

Figure captions

Figure 1: Sample localities: a) regional map showing the locations of Ischia and of the distal sample localities; b) Schematic map of Ischia showing the outcrop of rocks of different ages on the island (modified from Di Napoli et al., 2011; after Della Seta et al., 2011). And of proximal sample localities: 1 – Sant’Angelo peninsula; 2 – Grotta di terra; 3 – Cavone dei Camaldoli; 4 – Monte Vezzi; 5 – Monte Cotto; 6 – Citara Poseidon; 7 – Punta Imperatore (see figure 1 for sample locations).

Figure 2: Diagnostic major element glass data for investigated proximal units on Ischia spanning ~39-75 ka compared to the compositional fields of glass data sets from the other Neapolitan volcanic centres of Campi Flegrei (Tomlinson et al., 2012) and Vesuvius (Tomlinson et al., submitted). Errors are 2 s.d. calculated using replicate analyses of MPI-DING ATHO-G.

Figure 3: Major element biplots of proximal Ischia tephra from the Pre-MEGT (red, a-c), MEGT (green, d-f) and Post-MEGT (blue, g-i). Green field denotes MEGT composition. Errors are 2 s.d. calculated using replicate analyses of MPI-DING ATHO-G.

Figure 4: trace element biplots of proximal Ischia tephra from the Pre-MEGT (red, a-c), MEGT (green, d-f) and Post-MEGT (blue, g-i). Green field denotes MEGT composition. Errors are smaller than symbols and are calculated as 2 s.d. of replicate analyses of MPI-DING ATHO-G.

Figure 5: Biplots comparing potential distal correlatives of MEGT from the Tyrrhenian, Ionian and Adriatic sea and from the southern Italian mainland (see table 5 for references). Errors are 2 s.d. calculated using replicate analyses of MPI-DING ATHO, errors on trace element analyses are smaller than the data symbols.

Figure 6 Map showing locations and thicknesses (where available) of MEGT tephra and the inferred isopach thicknesses used for calculating the volume of MEGT tephra. Grey symbols indicate locations where chemical data is available, open symbols are locations of tephra correlated to Y-7, C-18 or MEGT but unconfirmed by this study (see table 5 for references).

Figure 7: Major and trace element biplots of Pre-MEGT tephra from Lago Grande di Monticchio (black symbols) compared to proximal Pre-MEGT tephra (red). Errors are 2 s.d. calculated using replicate analyses of MPI-DING ATHO-G, trace element errors are smaller than the data symbols.

Figure 8: Major and trace element compositions of LGdM tephra normalised to the average composition of the potential equivalent Pre-MEGT proximal tephra. The range of proximal compositions is given by the grey field. Plots exclude MnO, P₂O₅, which are close to the limit of detection and thus have poor precision in EMPA and also Sr and Ba, which are affected by microlite analysis in LA-ICP-MS.

Figure 9: (a-d) Major and trace element biplots of Post-MEGT tephra from Lago Grande di Monticchio (black symbols) compared to proximal Post-MEGT tephra (blue). Errors are 2 s.d. calculated using replicate analyses of MPI-DING ATHO-S. (e-f) Major and trace element compositions of LGdM tephra normalised to the average composition of the potential proximal Post-MEGT equivalent, the range of proximal compositions is given by the grey field. Plots exclude MnO, P₂O₅, which are close to the limit of detection and thus

have poor precision in EMPA and also Sr and Ba, which are affected by microlite analysis in LA-ICP-MS.

Figure 10: Correlations between the proximal Ischia stratigraphy (modified after Brown et al., 2008, K-Ar ages from Vezzoli 1988 and Poli et al. 1987) and the distal record at Lago Grande Di Monticchio (Wulf et al., 2004, 2012). Pre-MEGT tephra are in red, MEGT/TM-19 in green and post-MEGT in blue, with the youngest in light blue.

<i>Eruption</i>	<i>Age (ka)</i>	<i>Locality</i>	<i>Deposit description</i>	<i>Sample</i>	<i>Phenocrysts</i>	<i>Sample description</i>
Agnone	43 [§]	Punta Imperatore	Pyroclastic pumicious tuff	OIS 103E ²	Alk fsp , cpx, bt	Light grey, vesicular pumice
Pietre Rosse	46 [§]	Citara Poseidon	Pyroclastic pumicious tuff	OIS 103F ²	Alk fsp , bt	White, vesicular pumice
Schiappone	50 [§]	Monte Cotto Monte Vezzi	6m thick pumice fall overlain by >60m thick ignimbrite	SC-MEGT 0315 (light and dark clasts from ignimbrite) ³ SC-MEGT 0313 (fall) ¹ SC MEGT 0309	Alk fsp, plag, bt, cpx	White to grey, vesicular pumice
MEGT	51- 59*	Acquamorta Cavone dei Camaldoli	Extracaldera ignimbrite 0.5 m thick Extracaldera deposit comprising 8.5m basal fall overlain by 3.5 welded ignimbrite and capped by a lithic breccia	CF 191 (ignimbrite) ⁴ OIS 0319 (breccia) ³ OIS 0325 (ignimbrite) ¹ OIS 0333 (fall) ³ OIS 0321 (fall) ¹	Alk fsp, cpx, bt	Green to grey vesicular pumice Light to dark grey vesicular pumice Grey, poorly vesiculated pumice Orange/ buff coloured vesicular pumice Light-grey vesicular pumice
Porticello	-	Grotta di Terra	<4m thick deposit of pumice fall with thin ash beds	OIS 0320 (fall) ¹ OIS 0316 (fall) ³	Alk fsp, cpx, bt	Buff coloured vesicular pumice
Tisichiello	-	Grotta di Terra	7m thick sequence of interbedded pumice fall and ash-rich pyroclastic density currents.	OIS 0315 (fall) ³ OIS 0314 (fall) ³ OIS 0311 (fall) ³ OIS 0309 (fall) ¹	Alk fsp, plag, cpx, bt	Buff coloured vesicular pumice
Olummo	-	Grotta di Terra	6m thick sequence of interbedded pumice fall deposits and thin ash beds overlain by block and ash flow deposit	OIS 0318 (block and ash) ³ OIS 0305 (fall) ³ OIS 0302 (fall) ¹	Alk fsp, plag, cpx, bt	Buff to Light grey coloured vesicular pumices
Sant'Angelo	-	Sant' Angelo peninsula	Interbedded pumice fall deposits and thin ignimbrites overlain by thick lithic breccia.	OIS 0330 (Ignimbrite) ³ OIS 0326 (fall) ¹	Alk fsp, cpx, bt, neph,	Buff to light grey coloured vesicular pumices

Table 1

Tephra	Depth (cm)	Varve Age (Cal BP)	Thickness (mm)	Max grain size (µm)	Colour	Phenocrysts	Lithics
TM-17-1c	2372.8	34980	5	100	white	Kf, plg, cpx, bt	V
TM-18-9a	2992.0	41420	1.5	500	white-beige	Kf, cpx, bt, plg, ap	V
TM-18-9e	3005.2	42000	13	200	white-beige	Kf, plg, bt, cpx	V
TM-18-14a	3345.4	50260	1	700	grey-brown	Kf, plg, cpx, bt	V
TM-18-17a	3508.5	55620	5	400	beige	Kf, cpx, plg, bt	-
TM-19	3831.0	60060	332	1100	beige-green	Kf, bt, cpx, plg	V
TM-20	3923.8	61370	6	200	beige	Kf, bt, plg, cpx, ac, ti	V
TM-20-1b	4067.6	64140	8	300	beige	Kf, bt, cpx, plg, ap	V
TM-20-1c	4104.7	64470	3	230	grey-brown	Kf, bt, cpx, ap, ac	V
TM-20-5	4657.0	72940	20	150	beige	Kf, cpx, bt, plg	V
TM-21-2a	5236.2	80990	7.5	200	white	Plg, kf, cpx, bt, ap	V
TM-23-20a	6685.9	99140	24	310	white-ockre	Kf, plg, bt, cpx	V
TM-24-3b	7243.6	103800	8	190	white	Kf, plg, cpx, bt, ap	-

Table 2

Analysis	Agnone	Pietre Rosse	Schiappone			MEGT		Porticello	Tisichiello			Olummo		Sant'Angelo		
	OIS 103E-18	OIS 103F-17	SC-MEGT 0315I-1	SC-MEGT 0315g-15	OIS 0333-16	CF 319-6	OIS 0333-16	OIS 0320-6	OIS 0311-20	OIS 0315-9	OIS 0314-21	OIS 0302-6	OIS 0305-25	OIS 0318-28	OIS 0326-5	OIS 0330-3
Total	95.63	94.73	94.27	96.79	96.15	95.83	96.15	95.44	95.57	97.99	96.59	96.81	93.53	93.46	96.51	96.10
SiO ₂	62.87	62.63	62.03	60.11	62.15	62.55	62.64	61.81	61.83	61.67	61.54	60.85	62.14	61.93	61.95	61.75
TiO ₂	0.56	0.46	0.50	0.55	0.50	0.49	0.62	0.56	0.55	0.58	0.52	0.61	0.49	0.62	0.65	0.56
Al ₂ O ₃	18.35	18.37	18.42	18.84	18.24	18.22	18.71	18.75	18.80	18.75	18.29	18.77	18.44	18.74	18.69	18.44
FeO	2.47	2.27	2.40	3.62	2.60	2.72	2.34	2.51	2.56	2.73	2.75	2.80	2.51	2.75	2.36	2.68
MnO	0.19	0.23	0.18	0.15	0.24	0.08	0.25	0.29	0.14	0.29	0.33	0.32	0.19	0.18	0.22	0.26
MgO	0.33	0.24	0.30	0.80	0.30	0.54	0.24	0.28	0.36	0.35	0.25	0.28	0.40	0.51	0.39	0.36
CaO	1.33	1.18	1.40	2.52	0.74	1.53	0.88	1.12	1.31	1.15	0.99	1.02	1.32	1.30	1.24	1.09
Na ₂ O	6.44	7.45	6.78	4.94	8.22	5.72	8.03	7.26	6.91	7.19	8.51	8.49	7.01	6.49	7.22	7.91
K ₂ O	6.79	6.42	7.39	7.96	6.15	7.77	5.77	6.68	6.92	6.53	5.92	6.00	6.87	6.91	6.64	6.16
P ₂ O ₅	0.06	0.04	0.07	0.17	0.03	0.12	0.04	0.05	0.10	0.09	0.04	0.09	0.05	0.07	0.03	0.09
Cl	0.62	0.71	0.53	0.35	0.83	0.27	0.49	0.69	0.51	0.68	0.85	0.77	0.58	0.51	0.60	0.71
V	32	23	36	79	25	42	25	27	31	31	23	28	25	28	33	25
Rb	422	343	334	247	516	259	516	526	310	459	550	570	539	245	482	531
Sr	4.4	<LOD	20.6	392	<LOD	36	<LOD	10.4	15.5	10.2	1.7	2.3	5.3	135	10.4	3.1
Y	51	48	38	24	72	25	72	73	39	63	73	90	75	29	70	70
Zr	503	576	369	210	796	202	796	693	381	638	947	1057	887	305	875	761
Nb	85	91	60	35	123	38	123	111	64	106	143	158	147	49	123	124
Ba	3.6	<LOD	10.3	661	3.8	31.2	4	3.3	7.9	13.1	2.3	3.3	4.6	121	6.9	3.2
La	107	109	80	53	157	60	157	146	87	131	168	201	175	74	163	156
Ce	216	202	158	104	301	117	301	296	185	265	321	372	333	135	311	298
Pr	24	20	17	11	30	13	30	32	18	28	33	37	33	14	31	30
Nd	88	73	58	43	102	48	102	115	66	99	104	118	111	47	106	105
Sm	16.2	11.9	10.0	8.5	17.1	<LOD	17.1	22.0	11.0	17.8	14.5	19.8	21.9	8.6	16.6	17.4
Eu	1.4	0.9	1.4	1.9	1.0	1.5	1.0	<LOD	1.3	1.3	0.9	1.0	<LOD	1.9	1.1	0.9
Gd	12.5	8.8	9.2	6.1	12.6	6.9	12.6	13.4	9.0	13.0	12.8	14.4	13.4	6.2	13.3	12.2
Dy	10.2	8.0	7.0	4.8	11.8	5.1	11.8	13.5	7.9	11.3	11.8	13.9	13.5	5.3	11.9	11.7
Er	5.2	5.2	3.9	2.4	7.7	2.7	7.7	7.7	4.2	6.6	7.4	9.1	7.5	2.9	7.0	6.8
Yb	5.4	5.5	4.2	2.5	8.3	2.6	8.3	6.7	3.8	6.4	7.5	10.3	7.4	3.0	7.0	7.3
Lu	0.8	0.9	0.6	<LOD	1.1	<LOD	1.1	0.9	0.6	1.0	1.1	1.4	1.3	0.4	1.2	1.1
Ta	4.4	4.2	3.2	1.7	5.7	1.9	5.7	5.7	3.0	5.0	5.7	6.6	5.9	2.4	5.7	5.5
Th	38	43	22.7	13.1	52	14.1	52	45	26	42	59	78	60	20	61	52
U	13.0	14.2	7.8	4.6	15.7	4.3	15.7	14.1	7.9	13.3	18.0	23.1	18.1	6.3	18.0	16.1

Table 3

	Tephra	Chemical Groupings
	Pre-MEGT Stratigraphy	Pre-MEGT Groups
Stratigraphic order of sampled units	<i>Porticello Tephra</i>	
	OIS 0320 (fall)	Pre-MEGT Group 1b
	OIS 0316 (fall)	
	<i>Tisichiello Tephra</i>	
	OIS 0315 (fall)	Pre MEGT Group 1b and 2
	OIS 0314 (fall)	
	OIS 0311 (fall)	Pre-MEGT Group 1a
	OIS 0309 (fall)	
	<i>Olummo Tephra</i>	
	OIS 0318 (block and ash)	Pre-MEGT Group 1a
	OIS 0305 (fall)	Pre-MEGT Group 1b and 2
	OIS 0302 (fall)	Pre-MEGT Group 2
	<i>Sant'Angelo Tephra</i>	
	OIS 0330 (flow)	Pre-MEGT Group 2
	OIS 0326 (fall)	

Table 4

	Tephra	Chemical Groupings
	Post-MEGT Stratigraphy	Post-MEGT Groups
Stratigraphic order of sampled units	<i>Agnone Tuff</i>	
	OIS 103E-2	Post-MEGT Group 1
	<i>Pietre Rosse Tuff</i>	
	OIS 103F ²	Post-MEGT Group 2
	<i>Schiappone Tephra</i>	
	SC-MEGT 0315 (light and dark clasts from ignimbrite) ³	Post-MEGT Group 1
	SC-MEGT 0313 (fall) ¹	
SC MEGT 0309 (fall)		

Table 5

LGM layer	TM-17-1c	TM-17-1c	TM-18-9a	TM-18-9a	TM-18-9e	TM-18-14a	TM-18-14a	TM-18-14a	TM-18-17a	TM-18-17a	TM-19	TM-19	TM-19	TM-19	TM-20	TM-20-1b	TM-20-1c	TM-20-5	TM-21-2a	TM-23-20a	TM-24-3b
analysis	15	20	1	7	6	11	9	17	19	17	14	20	43	25	3	1	8	7	2	14	13
sum	90.84	94.03	93.91	95.34	98.16	92.28	93.06	96.81	92.56	93.49	96.14	98.08	96.77	95.97	94.89	95.71	99.83	99.12	96.60	98.35	97.64
SiO ₂	62.44	62.88	63.38	62.98	63.04	62.35	62.57	62.32	62.72	62.13	62.05	61.75	61.97	62.64	62.05	62.35	61.96	61.34	62.49	61.84	62.08
TiO ₂	0.44	0.48	0.43	0.50	0.46	0.42	0.47	0.41	0.42	0.44	0.57	0.59	0.55	0.56	0.62	0.60	0.61	0.57	0.55	0.57	0.71
Al ₂ O ₃	18.46	18.34	18.47	18.65	18.20	18.74	18.63	18.44	18.44	18.57	18.48	18.44	18.61	18.26	18.62	18.47	18.41	18.58	18.46	18.46	18.07
FeO	2.54	2.30	2.28	2.37	2.23	2.26	2.26	2.71	2.24	2.56	2.69	2.62	2.61	2.45	2.61	2.49	2.56	2.75	2.65	2.68	2.85
MnO	0.13	0.27	0.16	0.13	0.11	0.17	0.13	0.13	0.22	0.07	0.22	0.23	0.25	0.21	0.28	0.22	0.23	0.26	0.20	0.30	0.31
MgO	0.48	0.25	0.26	0.29	0.24	0.27	0.27	0.43	0.30	0.48	0.33	0.30	0.30	0.42	0.29	0.27	0.29	0.29	0.36	0.30	0.33
CaO	1.65	1.19	1.35	1.42	1.27	1.36	1.38	1.72	1.40	1.81	1.12	1.12	0.99	1.30	1.08	1.08	1.11	0.97	1.31	0.99	0.97
Na ₂ O	5.33	7.19	5.78	6.06	6.87	7.12	6.46	5.42	6.38	5.23	7.57	7.86	7.77	6.84	7.37	7.24	7.55	8.49	6.37	7.96	7.87
K ₂ O	8.07	6.36	7.31	6.96	6.84	6.50	7.06	7.95	7.25	8.17	6.14	6.27	6.20	6.66	6.32	6.51	6.59	5.90	7.07	5.99	6.01
P ₂ O ₅	0.09	0.05	0.04	0.06	0.02	0.09	0.04	0.09	0.05	0.13	0.05	0.05	0.05	0.08	0.05	0.06	0.04	0.03	0.04	0.03	0.03
Cl	0.36	0.70	0.55	0.59	0.71	0.71	0.72	0.37	0.59	0.40	0.78	0.75	0.69	0.57	0.71	0.70	0.63	0.82	0.51	0.87	0.77
V	45	25	26	36	26	28	32	45	35	49	28	25	32	35	28	27	26	23	33	<LOD	<LOD
Rb	260	447	343	349	388	422	375	252	322	255	503	424	360	286	474	444	458	551	314	553	540
Sr	100.2	4.1	16.5	24.7	4.9	13.8	9.6	101.3	23.7	99.7	4.4	3.8	6.0	15.5	4.1	6.0	3.0	2.1	<LOD	<LOD	<LOD
Y	24	51	31	40	48	44	42	26	35	25	68	67	45	30	63	63	65	75	43	78	76
Zr	217	599	335	419	500	557	452	222	345	219	789	645	391	258	651	605	612	875	407	1024	946
Nb	38	92	59	67	81	88	77	37	56	36	123	110	71	46	110	104	107	136	67	144	144
Ba	81.4	9.2	15.1	24.9	2.2	13.2	9.3	83	18.9	78	12.0	11.1	5.1	10.8	4.8	7.4	3.7	5.2	<LOD	<LOD	8.9
La	53	116	69	86	100	109	90	55	76	55	149	129	92	68	138	127	134	164	92	182	193
Ce	103	216	133	167	195	205	177	107	150	108	290	258	189	135	265	260	272	321	184	327	355
Pr	11	21	14	18	20	20	18	12	15	11	30	28	20	14	28	27	28	30	19	31	34
Nd	41	70	49	63	70	67	67	43	60	41	102	102	75	55	98	95	96	104	71	101	114
Sm	7.3	11.9	<LOD	11.8	12.1	12.2	12.0	8.1	10.1	7.1	17.2	20.4	16.4	10.6	16.7	16.2	16.9	16.4	<LOD	15.4	17.1
Eu	1.6	<LOD	<LOD	1.4	1.1	<LOD	1.2	1.5	1.3	1.6	0.9	0.9	1.3	1.3	1.0	1.0	1.2	0.9	<LOD	<LOD	<LOD
Gd	5.6	8.6	<LOD	8.2	9.5	8.6	9.3	6.0	8.0	5.7	13.8	12.4	10.4	6.7	12.3	12.2	12.0	14.6	<LOD	11.6	13.3
Dy	4.5	8.5	5.8	7.3	8.1	8.1	7.6	5.1	6.9	4.5	12.5	11.8	8.1	6.4	12.1	11.4	11.8	12.8	<LOD	11.3	12.5
Er	2.5	5.2	3.1	4.0	4.7	4.6	4.0	2.6	3.5	2.6	6.8	6.2	4.6	3.2	6.7	6.1	6.5	7.0	<LOD	7.9	7.7
Yb	2.5	5.7	3.3	4.1	4.9	5.2	4.5	2.7	3.6	2.1	8.0	5.4	4.0	3.0	6.9	6.1	6.6	7.8	<LOD	8.1	8.7
Lu	<LOD	0.8	<LOD	0.6	0.8	0.8	0.7	<LOD	0.5	0.4	1.0	0.9	0.6	0.4	1.0	0.9	1.0	1.1	<LOD	<LOD	<LOD
Ta	1.9	4.0	2.9	3.6	4.3	4.3	3.6	2.0	2.8	1.8	5.5	5.4	3.6	2.5	5.4	5.1	5.1	6.0	<LOD	5.9	6.2
Th	14	44	22	30	35	38	30	15	22	14	53	37	27	18	45	41	43	59	28	69	76
U	4.5	13.8	7.8	9.2	11.7	12.7	9.9	4.5	6.8	4.1	15.8	11.6	7.4	5.3	14.0	12.5	12.7	19.1	8.5	24	23

Site	Location	Layer	Thickness (cm)	Direction	Reference
<i>Core</i>					
PRAD 1-2	Adriatic sea	1870 cm	crypto	NNE	Bourne et al, 2010
KET 82-18	Adriatic sea	C-18	unknown	ENE	Paterne et al., 1988
M25/4-11	Ionian Sea	Y-7	4cm	SE	Keller et al., 1994, 1978; Kraml 1997
M25/4-10	Ionian Sea	Y-7	>2cm [§]	SE	Keller et al., 1994
M25/4-12	Ionian Sea	Y-7	3.5-4 cm	SE	Keller et al., 1994
M25/4-13	Ionian Sea	Y-7	4.5 cm	SE	Keller et al., 1994
RC9-190	Ionian Sea	Y-7	unknown	SE	Keller et al., 1978
RC9-191*	Ionian Sea	Y-7	unknown	SE	Keller et al., 1978
V10-68	Ionian Sea	Y-7	unknown	SE	Keller et al., 1978
KC01B	Ionian Sea	tephra 14	unknown	SE	Lourens, 2004
KET 8003*	Tyrrhenian Sea	C-18	unknown	SSE	Paterne et al., 1988
KET 8011	Tyrrhenian Sea	C-18	unknown	S	Paterne et al., 1988
MD01_2474G	Tyrrhenian Sea	MD28	11	S	Tamburrino, 2008
ODP Leg 107-650*	Tyrrhenian Sea	T003	3.5	S	Calanchi et al. 1994, McCoy and Cornell 1990
KET 8004*	Tyrrhenian Sea	C-18	20	SSW	Paterne et al., 1986, 1988
KET 8022*	Tyrrhenian Sea	C-18	unknown	W	Paterne et al., 1988
Lago Grande di Monticchio	Southern Italy	TM-19	32 (2 cm fall)	E	Wulf et al., 2004
San Gregorio Magno*	Southern Italy	S16	10	E	Munno and Petrosino 2007
<i>Outcrop</i>					
Val d'Agri	Southern Italy	T3D4	18	ESE	Zembo et al., 2011
Stromboli	Aeolian Islands	IT	25-30	SSE	Morche 1988, Hornig- Kjarsgaard et al. 1993
Salina*	Aeolian Islands	IT	35-40	SSE	Keller 1969
Lipari	Aeolian Islands	IT	30-50	S	Lucchi et al 2008
Panarea	Aeolian Islands	IT	17	S	Lucchi et al 2008
Filicudi	Aeolian Islands	IT	30-50	S	Lucchi et al 2008

Bold, chemical data available (*major element only)

[§]core is cut through this layer so 2 cm is a minimum.

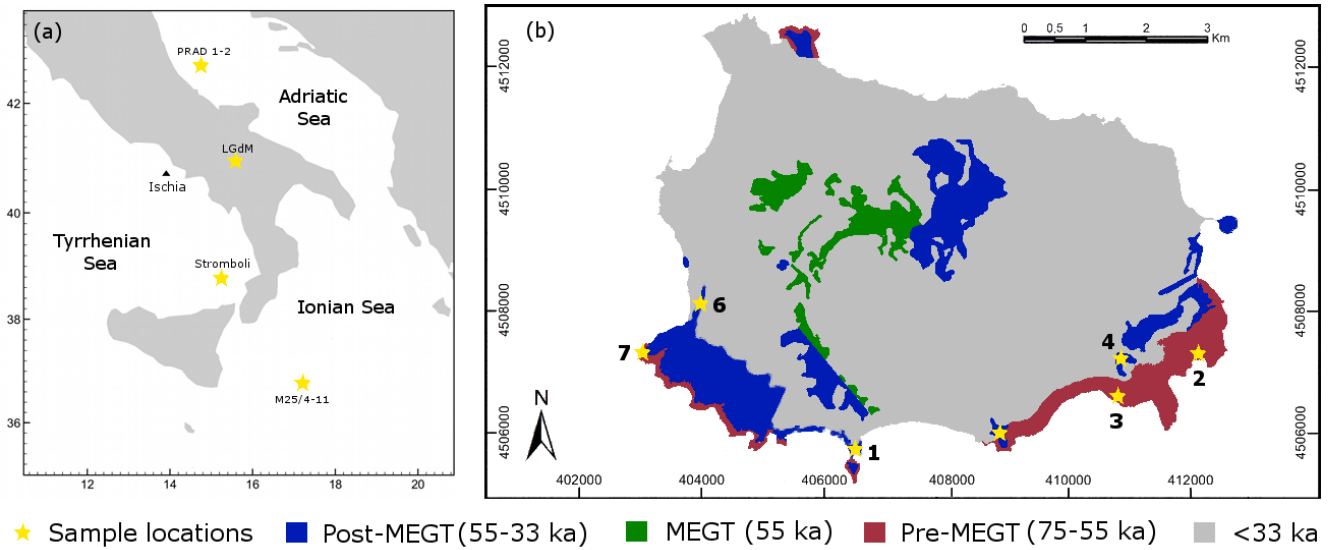


Fig 1

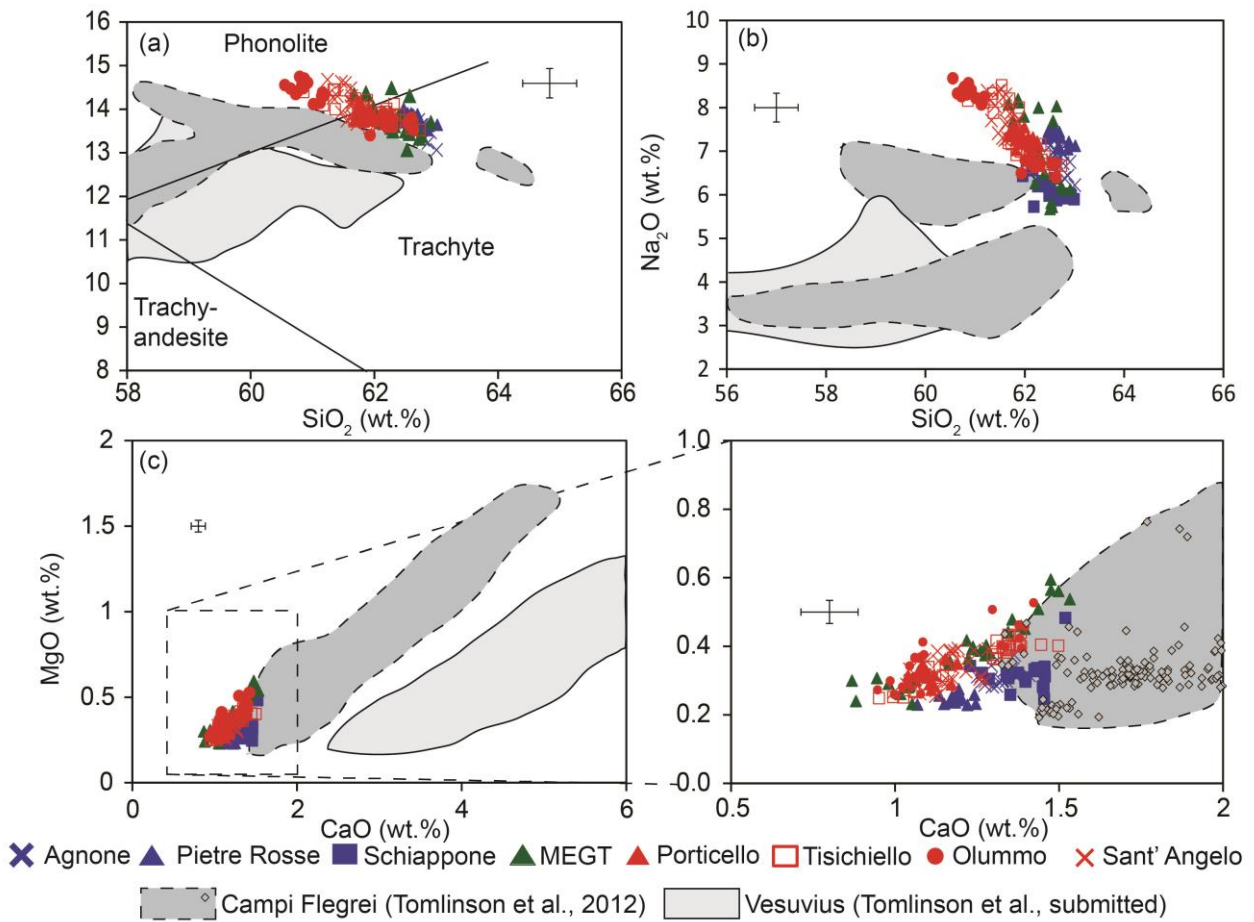


Fig 2

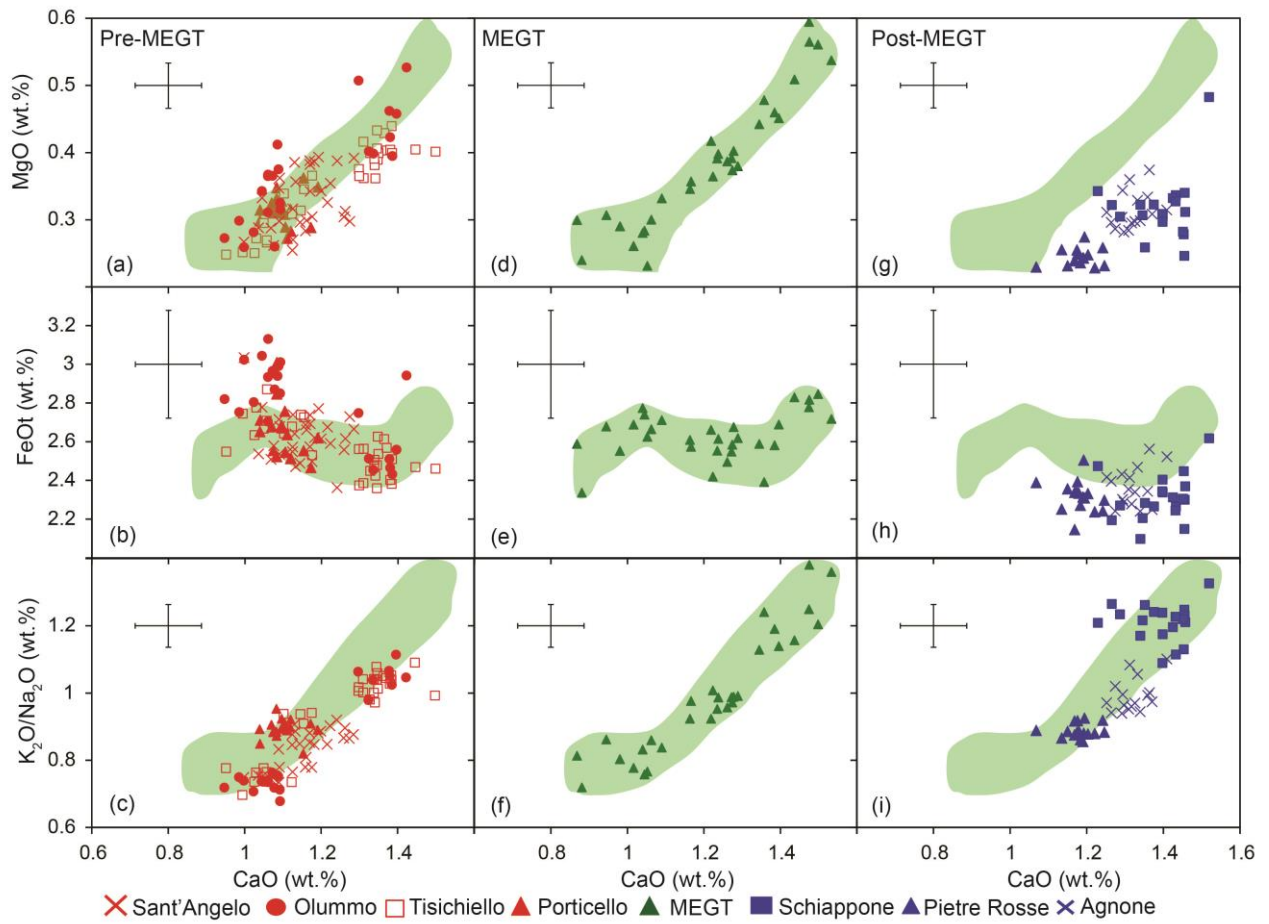


Fig 3

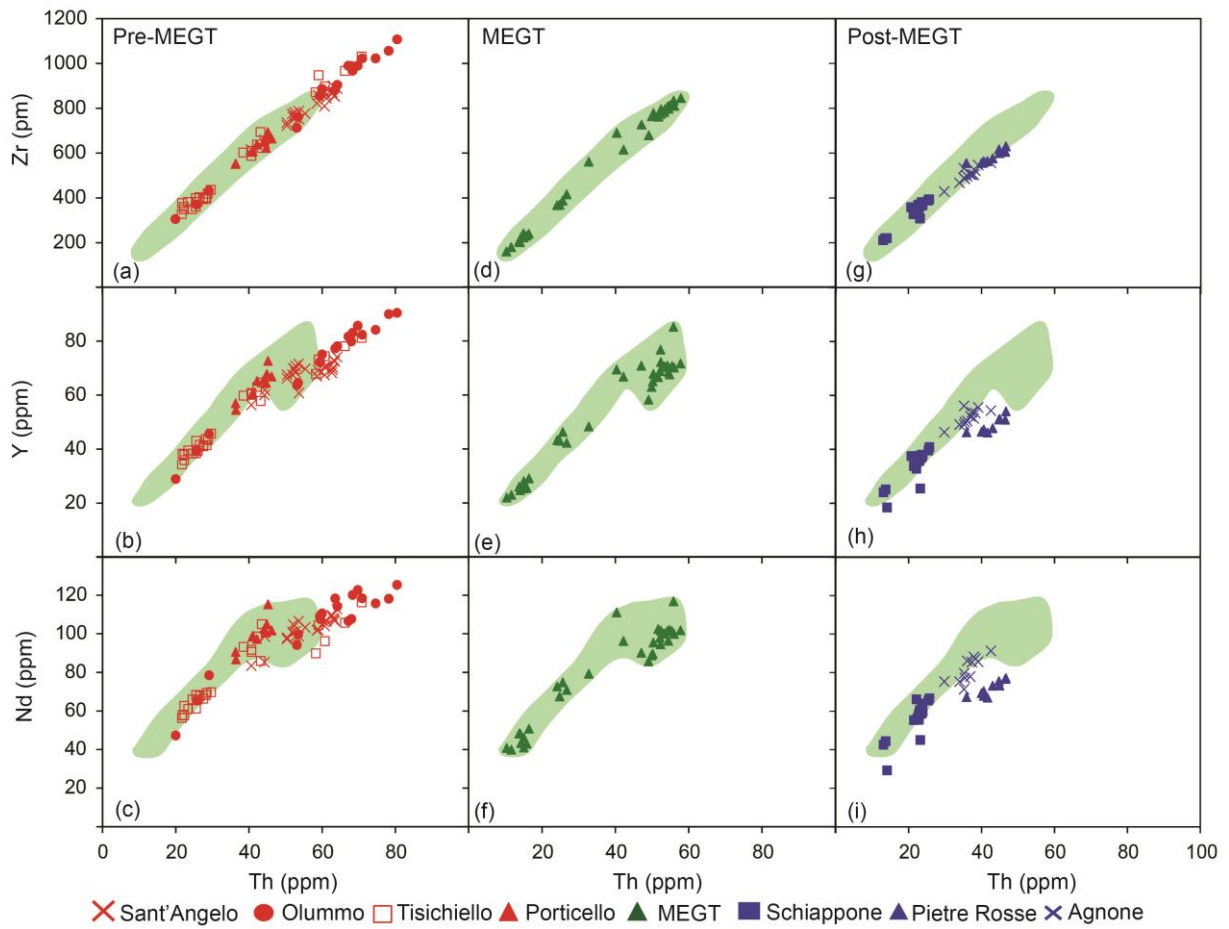


Fig 4

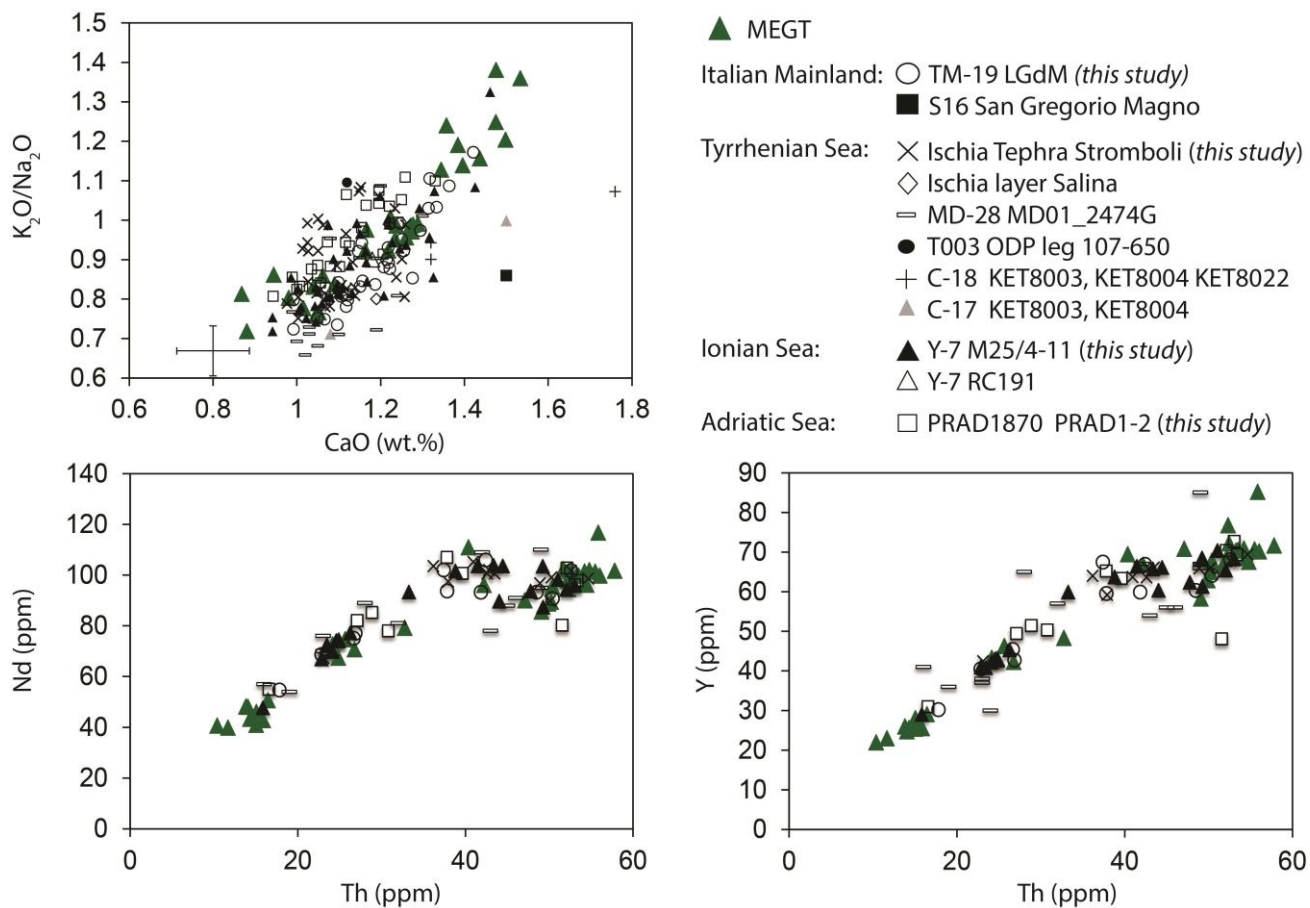


Fig. 5

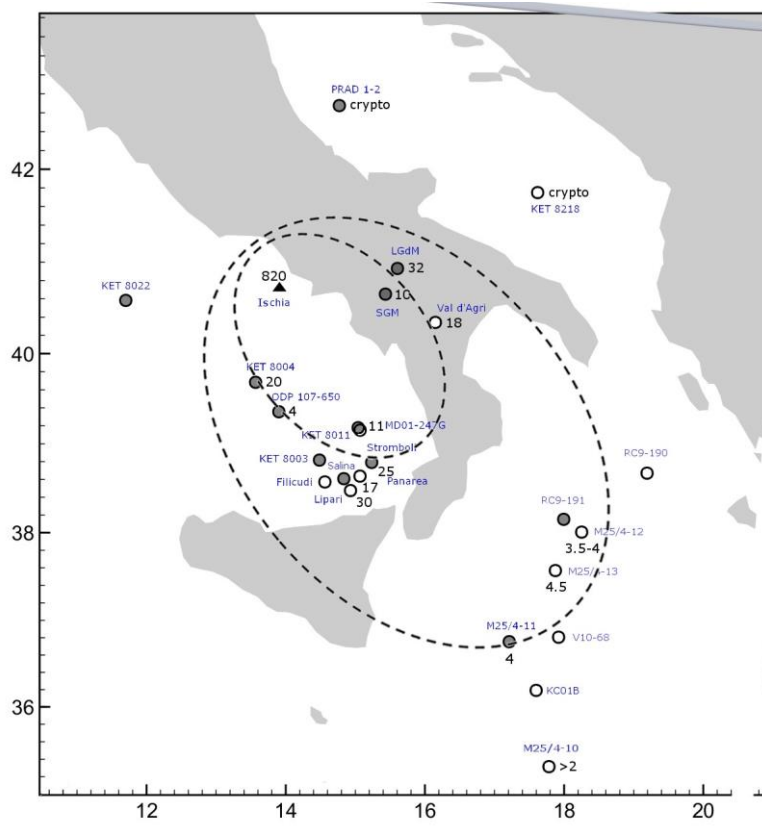


Fig 6

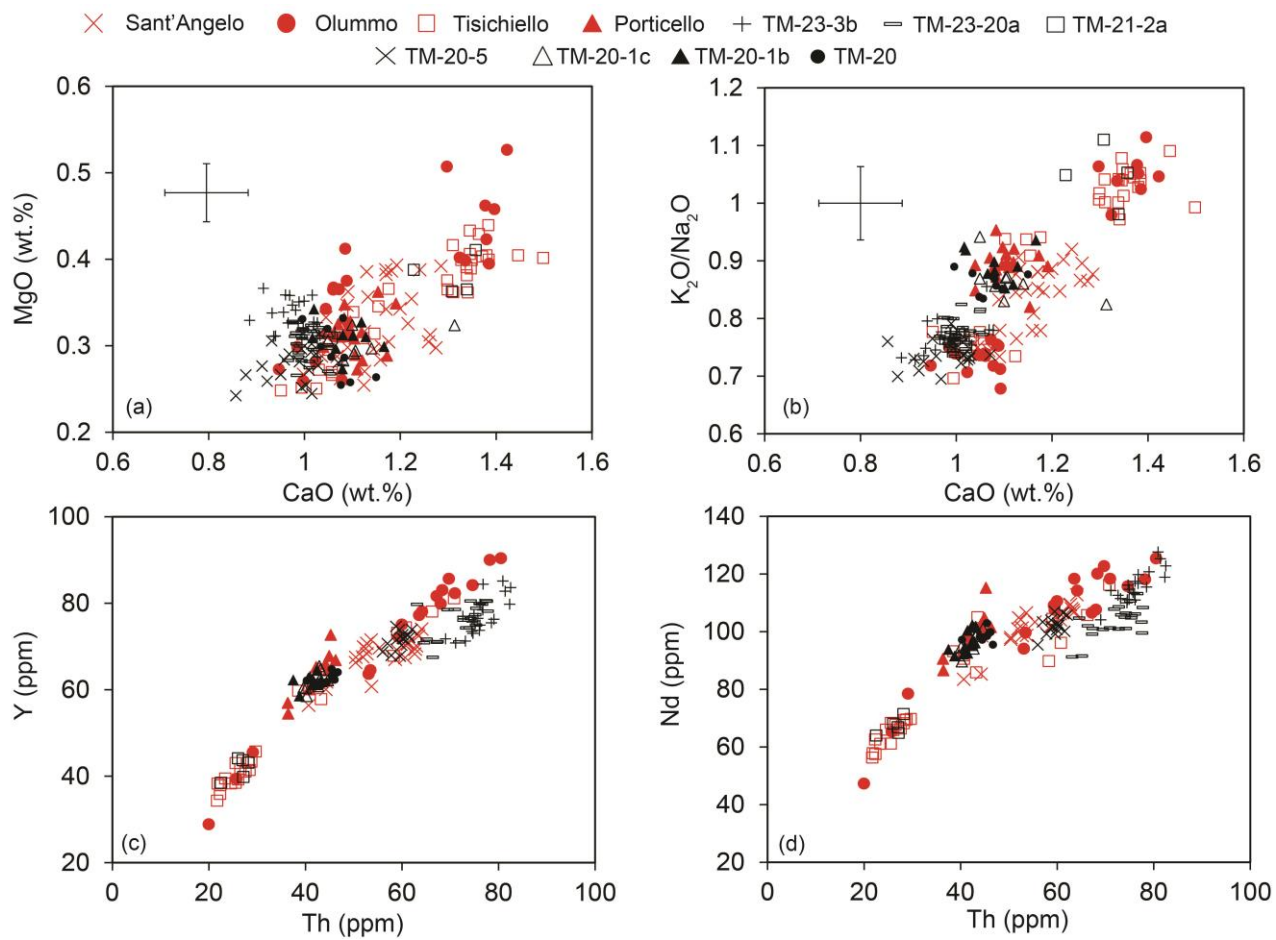


Fig 7

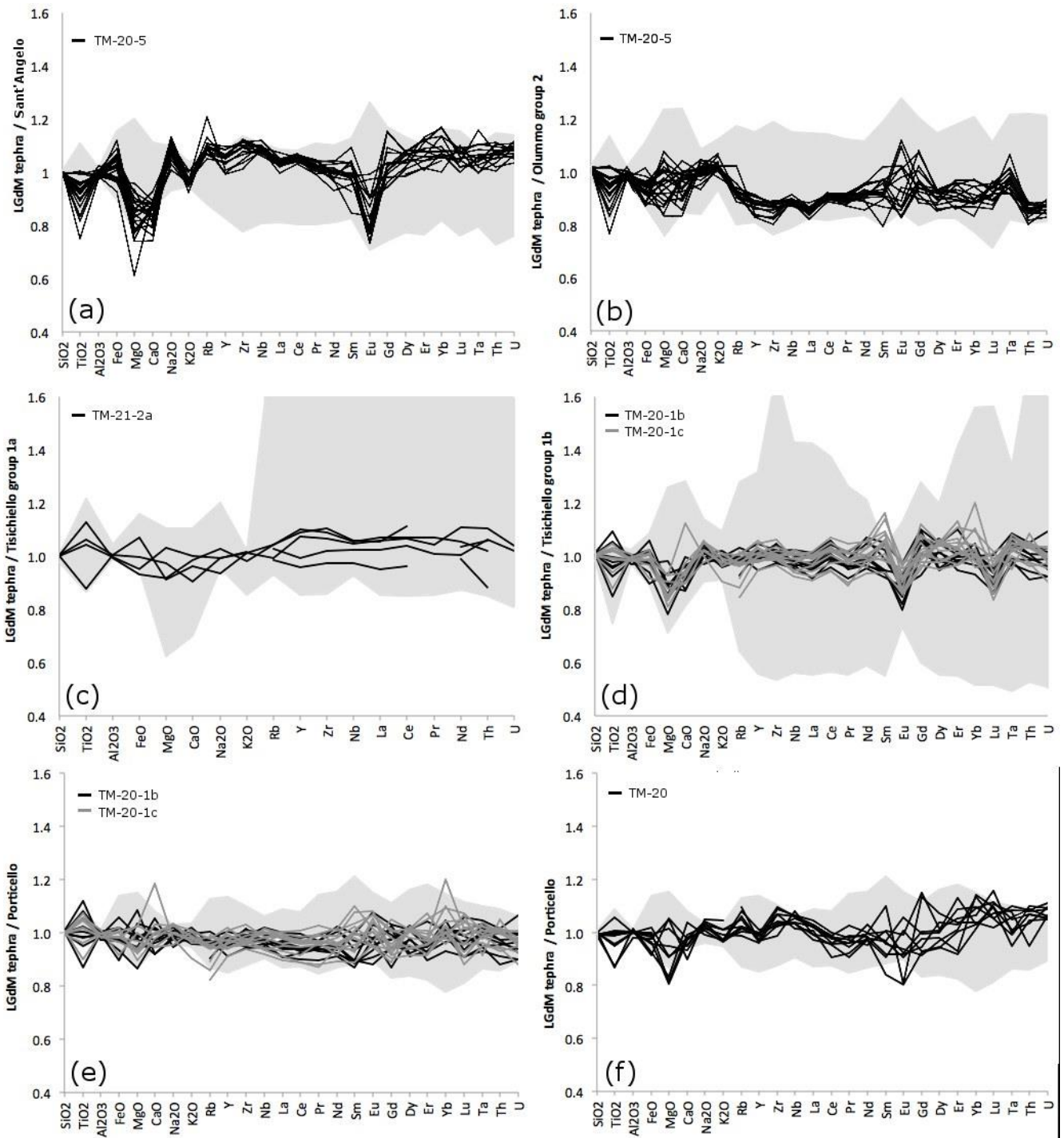


Fig 8

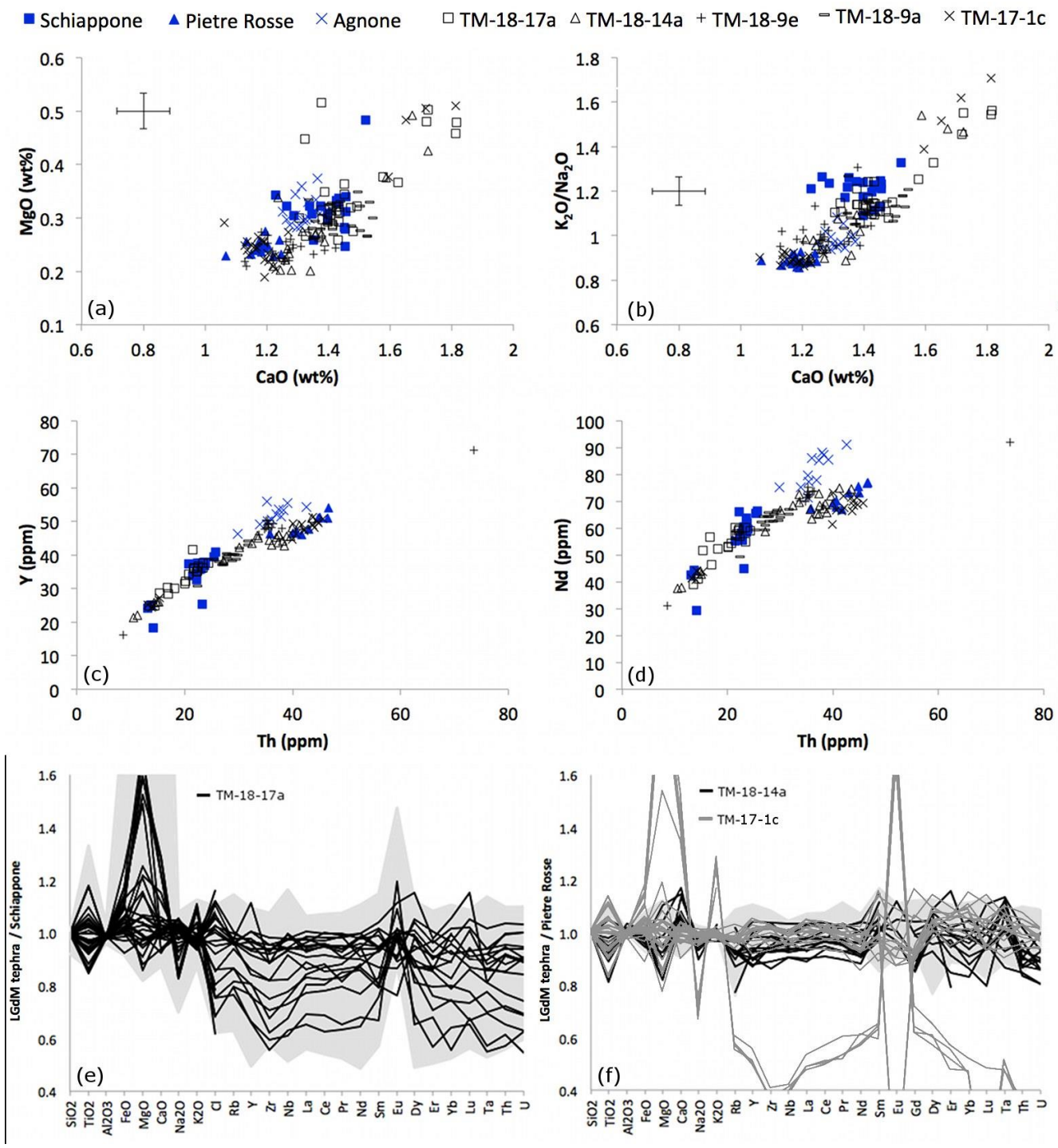


Fig. 9

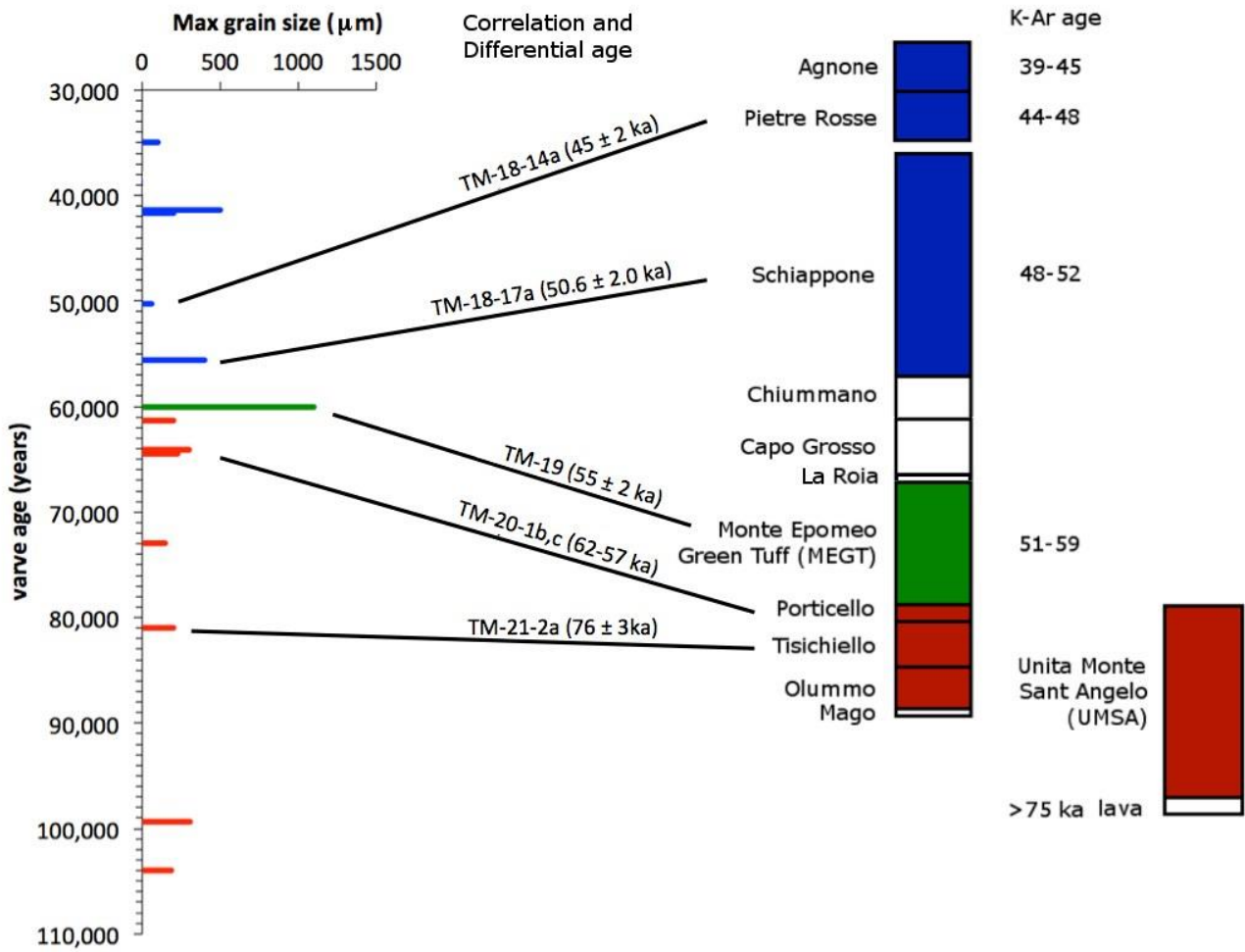


Fig 10